ORIGINAL RESEARCH

Nuclear Receptor Nur77 Protects Against Abdominal Aortic Aneurysm by Ameliorating Inflammation Via Suppressing LOX-1

Hengyuan Zhang, BS*; Na Geng, BS*; Lingyue Sun, MS*; Xinyu Che, MS; Qingqing Xiao, MS; Zhenyu Tao, MS; Long Chen, BS; Yuyan Lyu, MD, PhD; Qin Shao (iD), MD, PhD; Jun Pu, MD, PhD

BACKGROUND: Abdominal aortic aneurysm (AAA) is a life-threatening vascular disorder characterized by chronic inflammation of the aortic wall, which lacks effective pharmacotherapeutic remedies and has an extremely high mortality. Nuclear receptor NR4A1 (Nur77) functions in various chronic inflammatory diseases. However, the influence of Nur77 on AAA has remained unclear. Herein, we sought to determine the effects of Nur77 on the development of AAA.

METHODS AND RESULTS: We observed that Nur77 expression decreased significantly in human and mice AAA lesions. Deletion of Nur77 accelerated the development of AAA in mice, as evidenced by increased AAA incidence, abdominal aortic diameters, elastin fragmentation, and collagen content. Consistent with genetic manipulation, pharmacological activation of Nur77 by celastrol showed beneficial effects against AAA. Microscopic and molecular analyses indicated that the detrimental effects of Nur77 deficiency were associated with aggravated macrophage infiltration in AAA lesions and increased pro-inflammatory cytokines secretion and matrix metalloproteinase (MMP-9) expression. Bioinformatics analyses further revealed that LOX-1 was upregulated by Nur77 deficiency and consequently increased the expression of cytokines and MMP-9. Moreover, rescue experiments verified that LOX-1 notably aggravated inflammatory response, an effect that was blunted by Nur77.

CONCLUSIONS: This study firstly demonstrated a crucial role of Nur77 in the formation of AAA by targeting LOX-1, which implicated Nur77 might be a potential therapeutic target for AAA.

Key Words: abdominal ■ angiotensin II ■ aortic aneurysm ■ inflammation ■ macrophage ■ nuclear receptor

Abdominal aortic aneurysms (AAAs) are permanent and localized aortic dilations, defined as an aortic diameter greater than 3.0 cm or 1.5 times the expected normal diameter.[1] The risk factors for AAA include male sex, smoking, older age, ethnicity, atherosclerosis, hypertension, and family history. Although most AAAs are asymptomatic until rupture, the mortality rate is exceptionally high, even reaching 80% when rupture occurs. At present, surgical intervention is still the mainstay treatment of this complex multifactorial disease. Nevertheless, surgical intervention is not recommended until the aorta reaches a diameter of 5.5 cm in men and

5.0 cm in women, where the risk of rupture exceeds the risk of repair. However, no medication has been convincingly shown to slow AAA progression currently.[2] Patient management is a matter of monitoring and waiting until the aorta reaches a size where repair is indicated. That highlights an emergent need to understand better the molecular and cellular mechanisms involved in AAA formation and progression to improve clinical management and prognosis of individuals with AAA.

Pathological features of AAA formation and progression include extracellular matrix (ECM) degeneration, vascular smooth muscle cell apoptosis, and

CLINICAL PERSPECTIVE

What Is New?
- Our present study first demonstrated that Nur77 protected against Ang II-induced aortic aneurysms in mice.
- The absence of Nur77 increased macrophage infiltrating, which contributed to severe inflammation and increased MMP-9 expression.
- The beneficial effects of Nur77 were mediated by LOX-1. Nur77 binds to the promoter of LOX-1 and suppresses its transcription activity.

What Are the Clinical Implications?
- Our findings identify Nur77 as a potential therapeutic target for treating or preventing AAA.

Nonstandard Abbreviations and Acronyms

AAA	abdominal aortic aneurysm
Ang II	angiotensin II
ApoE	apolipoprotein E
BMDM	bone-marrow derived macrophage
ECM	extracellular matrix
LOX-1	lectin like Ox-LDL receptor-1
MMP	matrix metalloproteinase

inflammatory cell infiltration.[3] Vascular inflammation is the main initial factor of aortic aneurysm. In this process, immune cells, including lymphocytes, mast cells, and macrophages, infiltrate into the tissue, evoking a series of inflammatory response and accelerating ECM remodeling.[4] Particularly, macrophages have crucial roles in inflammatory response and ECM degradation.[5] Previous studies have shown the essential part of infiltrating macrophages in AAA, including matrix degradation, oxidative stress, and inflammation.[6–8] Therefore, regulating the function of macrophages could be crucial to reduce AAA formation.

Nur77 (also known as TR3, NGFI-B, and NR4A1), an orphan member of the nuclear receptor superfamily, is known to play an integral role in many different cellular processes, especially the inflammatory responses.[9,10] Inflammatory stimuli could induce the expression of Nur77 in human and mouse macrophages.[11,12] In turn, Nur77 restricts inflammatory response via inhibiting NF-κB signaling in macrophages. Our previous studies revealed that Nur77 suppressed apoptosis and pro-inflammatory cytokines in macrophages.[13,14] Moreover, accumulating evidence suggests that Nur77 is involved in inflammatory vascular diseases, such as atherosclerosis, cardiac hypertrophy, and cardiac ischemia/

reperfusion injury.[15–17] However, whether Nur77 is involved in AAA has not yet been investigated.

In this study, we found that the expression of Nur77 was decreased in human and mice AAA lesions. Furthermore, we used mice genetically deficient in Nur77 to elucidate the underlying molecular mechanism of how Nur77 participated in Ang II-induced AAA formation in mice.

METHODS

Additional details are provided in Data S1. The data that support the findings of this study are available from the corresponding author upon reasonable request. Key reagents and resources are described in Table S1.

Animal Experiment

The animal protocol was reviewed and approved by the Animal Ethics Committee of Renji Hospital (RJ2018-1012) and all mouse experiments conform to the National Institutes of Health (NIH) Guidelines for the Care and Use of Laboratory Animals. We utilized a CRISPR/Cas9 strategy to yield Nur77 knockout mice. ApoE$^{-/-}$ mice were obtained from the Shanghai Model Organisms Center, Inc. Nur77$^{-/-}$ mice were crossed with AopE$^{-/-}$ mice to generate ApoE$^{-/-}$Nur77$^{-/-}$ mice. ApoE$^{-/-}$ and ApoE$^{-/-}$Nur77$^{-/-}$ mice (6–8 weeks males) on the C57BL/6 background were used for the experiments.

Angiotensin II(Ang II)-induced AAA was established as previously described.[18] Briefly, mini-osmotic pumps (Model 2004, Alzet) were implanted subcutaneously in the right dorsum of each mouse to deliver Ang II (A9525, Sigma-Aldrich) at a rate of 1000 ng/kg/min or normal saline for up to 28 days. Mice were kept in micro-isolator cages on a 12-hour day/night cycle and were fed a high-fat diet.

In another set of experiments, to investigate the effect of celastrol on AAA, ApoE$^{-/-}$ mice were infused subcutaneously with Ang II or saline for 28 days. Ang II-infused ApoE$^{-/-}$ mice were randomly allocated to the following groups: (1) treatment with vehicle, (2) treatment with celastrol at a dose of 1 mg/kg/d. Celastrol or vehicle was administered by intraperitoneal injection every other day for 28 days. Similarly, saline-infused mice were intraperitoneally injected with vehicle or celastrol at the same dose. Celastrol (HY-13067, MedChemExpress) was dissolved in dimethyl sulfoxide (DMSO) to generate a stock concentration of 100 mg/ml, stored at −20°C. Celastrol was diluted with PBS or cell culture solution to the required concentration before usage.

Nur77$^{-/-}$ Mice Construction

Details are described in Supplemental Methods. The gRNAs sequence and primer information are provided

in Table S2. The baseline date of Nur77$^{-/-}$ mice is presented in Figure S1.

Histomorphology Analysis

Details are described in Supplemental Methods. Representative images are shown in Figure S2.

Immunofluorescence Staining

Details are described in Supplemental Methods. Representative images are shown in Figure S2.

Quantitative Real-time PCR

Details are described in Supplemental Methods. The primers used for q-PCR are listed in Table S3.

Western Blot Analysis

Details are described in Supplemental Methods. The full blots of the western data are shown in Figure S3.

RNA Sequencing

Details are described in Supplemental Methods. QC metrics for the RNA-seq data are shown in Table S4. Principal component analysis (PCA) is presented in Figure S4.

Statistical Analysis

Statistical analyses were performed with GraphPad Software (Version 8.0). Data were presented as mean ± SEM of at least three independent experiments. The comparisons of AAA incidence were made by the Chi-square test. Student's t test was used for two-group comparisons. Multiple-group comparisons were carried out using one-way ANOVA with the Tukey or Dunnett's T3 (unequal variances) post hoc test; and two-way ANOVA with the Tukey post hoc test. P-values <0.05 were considered to be significant.

RESULTS

Nur77 Expression is Downregulated in AAA Formation

To investigate whether Nur77 is involved in the pathogenesis of abdominal aortic aneurysm, we first detected the expression of Nur77 in human AAA tissue. The mRNA and protein levels of Nur77 were both downregulated compared to adjacent nonaneurysmal aortic sections (Figure 1A). Consistently, in Ang II-induced AAA mouse model, considerable reduction of Nur77 mRNA and protein were observed in Ang II–infused mice compared with the control mice (Figure 1B). Moreover, double immunofluorescence staining of AAA tissues showed that CD68-expressing

cells co-expressed Nur77 (Figure 1C), which suggested that Nur77 within macrophages may play a critical role in AAA.

We next verified whether Ang II influenced Nur77 in macrophages in vitro. We followed Nur77 expression stimulated by Ang II using q-PCR and Western blot. Nur77 mRNA level increased after 30 minutes and reached a plateau at 1 hour. Then the expression of Nur77 decreased in a time-dependent manner (Figure 1D). This change in Nur77 mRNA was followed by a decrease in protein (Figure 1E). Moreover, Nur77 staining was markedly decreased in macrophages after Ang II stimulation (Figure 1F). The altered Nur77 levels implied a potential role of Nur77 in AAA pathogenesis.

Nur77 Deficiency Aggravates Ang II-Induced AAA Formation

To understand better the role of Nur77 in AAA pathogenesis, we subjected ApoE$^{-/-}$ and ApoE$^{-/-}$Nur77$^{-/-}$ mice to AAA surgery. As depicted in Table S5, Ang II infusion increased blood pressure without affecting the heart rate. Morphologically, none of the ApoE$^{-/-}$ and ApoE$^{-/-}$Nur77$^{-/-}$ mice (10 mice per group) showed evidence of AAA when infused with saline (Figure 2A). The incidence of Ang II-induced AAA in ApoE$^{-/-}$ mice was 60% (18/30). In contrast, 83% (25/30) of ApoE$^{-/-}$Nur77$^{-/-}$ mice developed AAA (Figure 2B). Additionally, the maximal aortic diameter and the ratio of total aortic weight to body weight was higher in Ang II-infused ApoE$^{-/-}$Nur77$^{-/-}$ mice than those in ApoE$^{-/-}$ mice (Figure 2C). To monitor the aortic enlargement and detect the internal diameter of suprarenal aortic non-invasively, we performed Magnetic Resonance Imaging (MRI) and color Doppler ultrasound imaging. Similarly, the maximal internal diameters were more extensive in ApoE$^{-/-}$Nur77$^{-/-}$ mice compared to ApoE$^{-/-}$mice (Figure 2D and 2E). We also subjected ApoE$^{-/-}$Nur77$^{+/-}$ mice to AAA surgery, the results revealed that the difference in AAA incidence is not significant compared to ApoE$^{-/-}$ mice (Figure S5).

Furthermore, the H&E staining showed that Nur77 deletion increased the aortic diameter after Ang II infusion (Figure 2F). Markedly, the ApoE$^{-/-}$Nur77$^{-/-}$ mice displayed aggravated collagen deposition and degradation of elastic laminas compared to ApoE$^{-/-}$ mice. These findings indicated that the absence of Nur77 could exacerbate AAA.

Nur77 Agonist Alleviates Ang II-Induced AAA Formation

Celastrol is a predominantly active natural product extracted from the Chinese herb *Tripterygium wilfordii* Hook.f. It has been reported that celastrol is a Nur77
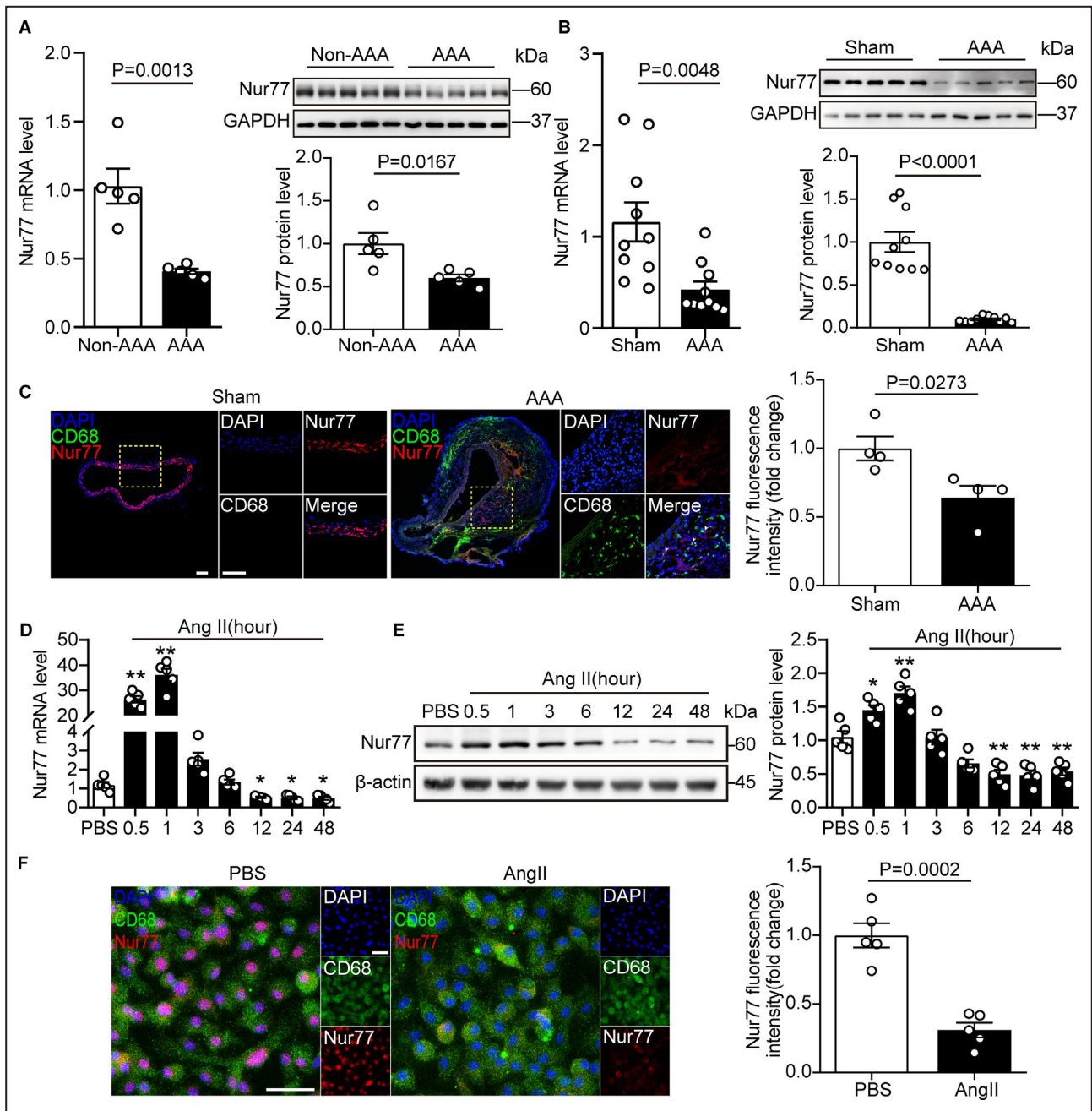
Figure 1.   Nur77 expression is downregulated in AAA formation
A, The relative mRNA and protein levels of Nur77 in human aneurysmal lesions and adjacent nonaneurysmal aortas (n=5 samples per group). **B,** The relative mRNA and protein levels of Nur77 in the abdominal aorta tissue from mice with AAA and sham control (n=10 mice per group). **C,** Representative images of dual immunofluorescence staining of Nur77 (red) and CD68 (green) in the abdominal aorta tissue from mice with AAA and sham control (n=4 per group). Scale bar indicates 100 μm. **D** and **E,** The relative mRNA and protein levels of Nur77 in Raw264.7 cells after stimulated with Ang II (1 μM) for the indicated time (n=5 per group, *P<0.05 vs PBS, **P<0.01 vs PBS). **F,** Representative images of dual immunofluorescence staining of Nur77 (red) and CD68 (green) in Raw264.7 cells and the relative quantification (n=5 per group). Scale bar indicates 50 μm. Data are presented as mean± SEM. Student's two-tailed *t* test for A, B, C, and F. One way-ANOVA followed by Dunnett's T3 multiple comparisons test for D, Tukey's multiple comparisons test for E. AAA, abdominal aortic aneurysm; Ang II, angiotensin II; PBS, phosphate buffered saline.

agonist that binds Nur77 to inhibit inflammation.[19] To dissect the in vivo effects of celastrol treatment in AAA, celastrol (1 mg/kg) or vehicle were administered by intraperitoneal injection, as described previously.[20]

Celastrol administration did not provoke changes in the systolic blood pressure in ApoE^{-/-} mice (Table S6). In the Ang II-infused group, 64% (16/25) of the group developed aneurysms. Treatment with celastrol reduced
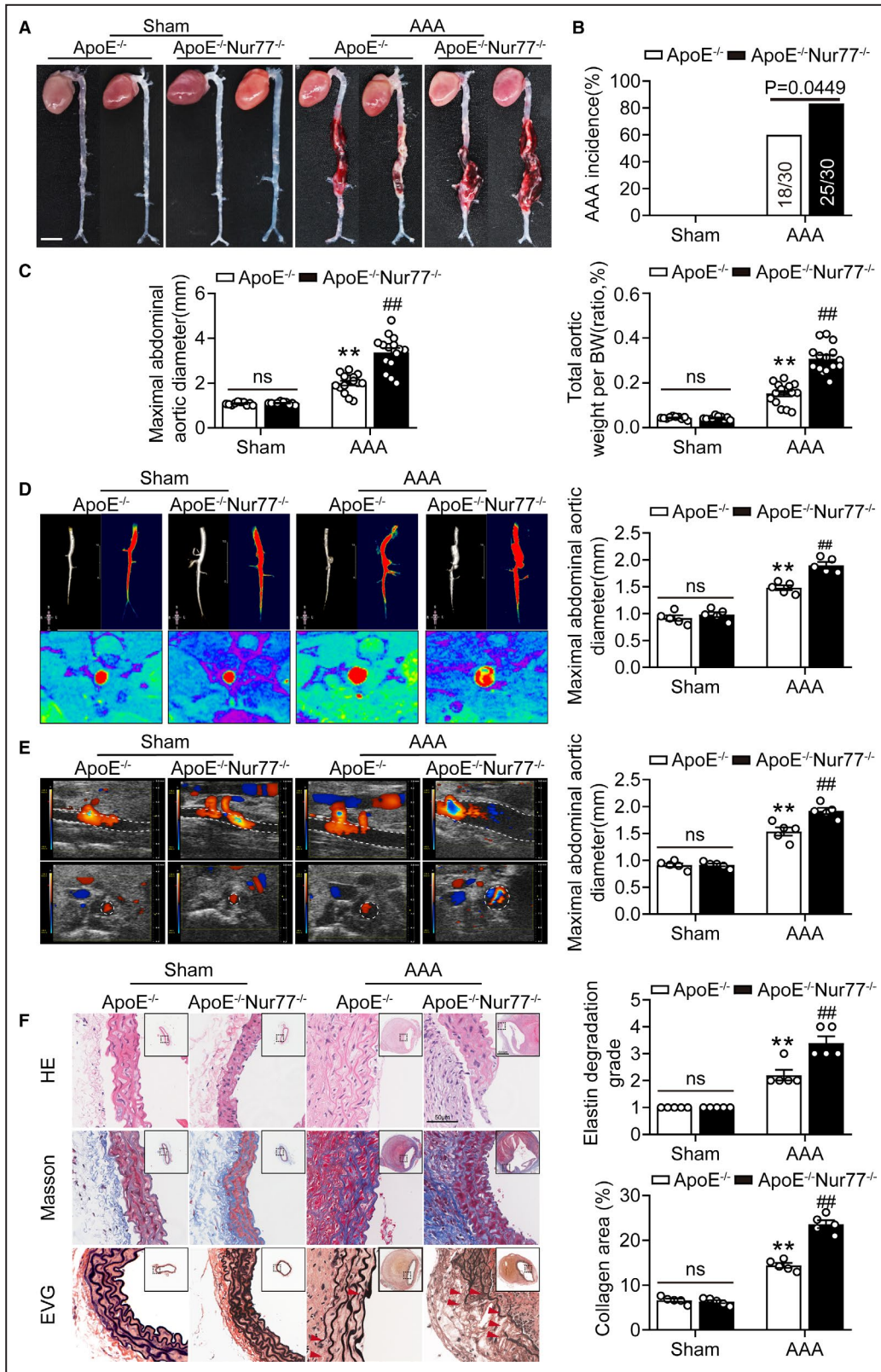
aneurysm formation to 32% (8/25) (Figure 3A and 3B). As expected, celastrol robustly reduced the maximal abdominal aortic diameter and total aortic weight (Figure 3C). MRI and color Doppler ultrasound imaging showed that celastrol reduced the maximal aortic diameter in mice (Figure 3D and 3E). Histological

Figure 2. Nur77 deficiency aggravates Ang II-induced AAA formation

A, Representative photographs showing mouse aortas infused with saline or Ang II at 4 Weeks. Scale bar indicates 5 mm. **B,** The incidence of AAA of the Ang II-infused mice compared with their sham controls. n=10 in each group of ApoE$^{-/-}$, ApoE$^{-/-}$Nur77$^{-/-}$ mice infused with saline, n=30 each for ApoE$^{-/-}$, ApoE$^{-/-}$Nur77$^{-/-}$ mice infused with Ang II. **C,** Maximal abdominal aortic diameter, total aortic weight-to-BW ratio of the indicated groups (n=10–15). **D,** Serials in vivo MRI of abdominal aortic aneurysms (AAA) and corresponding transverse images, and the quantification of maximal abdominal aortic diameter. Red denotes 3D-reconstructed MRI images of the abdominal aorta (n=5 mice per group). **E,** Representative views of the internal diameter of the abdominal aorta measured with ultrasonography on day 28 after surgery and the quantification of the maximal abdominal aortic diameter (n=5 mice per group). **F,** Representative images of suprarenal aortic sections stained with hematoxylin and eosin (H&E), Masson Trichrome (collagen) and Van Gieson (elastin) after saline or Ang II infusion. The red arrows show the rupture of elastin fibers. Right panel shows the grade of elastin degradation and collagen deposition in the aortic wall of mice (n=5 per group). **P<0.01 vs Sham-ApoE$^{-/-}$ mice; ##P<0.01 vs AAA-ApoE$^{-/-}$ mice. Data are presented as mean± SEM. Chi-square test for B. Two-way ANOVA followed by Tukey's multiple comparisons test for C, D, E, and F. BW, body weight; ns, nonsignificant.

analysis demonstrated that mice injected with celastrol exhibited decreased aortic expansion (Figure 3F). Moreover, celastrol ameliorated collagen deposition and elastic lamina degradation. Collectively, these results suggested that Nur77 activation by celastrol-mitigated AAA formation.

Nur77 Deficiency Enhances AAA Lesion Macrophage Infiltration and Inflammatory Response

As macrophages infiltrating into aortic tissue and secreting matrix degradable substance contribute to AAA formation,[3] we sought to evaluate whether Ang II infusion gives rise to a heightened state of vascular inflammation in Nur77-deficient mice. The accrual of macrophages characterized by immunostaining directed against F4/80 was notably increased in ApoE$^{-/-}$Nur77$^{-/-}$ as opposed to ApoE$^{-/-}$ aortas from mice (Figure 4A). To gain further insights into the inflammatory response, we tested the expression of inflammation-related genes in the aortic. The results showed that mRNA expression of IL-1b, TNFα, CCL2, and IL-6 was increased in ApoE$^{-/-}$Nur77$^{-/-}$ mice (Figure 4B).

Matrix metalloproteinases (MMPs) play a crucial role in the formation and progression of AAA. In particular, VSMC-derived MMP2 and macrophage-derived MMP9 are critical for AAA development. Thus, we next determined whether Nur77 deletion affected the levels of MMP2 and MMP9 in Ang II-induced AAA formation. Western blots showed that Ang II infusion for 4 weeks upregulated the expressions of MMP-2 and MMP-9 in ApoE$^{-/-}$ mice. The deletion of Nur77 markedly increased MMP-9 expression, but not the MMP-2 expression (Figure 4C). Furthermore, Nur77 deletion also elevated gene expression of MMP-9 (Figure 4D). We also examined the MMP activity in vivo by using an in situ zymography assay. As shown in Figure 4E, Nur77-deletion increased MMP activity. Immunohistochemical staining demonstrated that the expression of MMP9 was immensely increased in Ang II-infused ApoE$^{-/-}$Nur77$^{-/-}$ mice (Figure 4A). By contrast, celastrol attenuated the macrophages infiltration and MMP-9 expression (Figure S6).

Nur77 deletion increases LOX-1 expression in abdominal aortas

We performed RNA-Sequencing on aorta tissues with aneurysms from ApoE$^{-/-}$ and ApoE$^{-/-}$Nur77$^{-/-}$ mice to interrogate further the role of transcription factor Nur77 in driving inflammatory vascular diseases. In total, the expression of 21878 mRNAs was detected, of which 358 genes had an adjusted $P<0.05$ in ApoE$^{-/-}$Nur77$^{-/-}$ mice as compared with ApoE$^{-/-}$ mice. Among them, 133 genes were upregulated, and 225 genes were downregulated (Figure 5A). Based on the KEGG analysis, we found that the PPAR signaling pathway displayed a significant change (Figure 5B).

To identify genes under the direct control of Nur77, we analyzed the Nur77 Chromatin immunoprecipitation and sequencing (ChIP-seq) dataset from GEO database (GSE102393), which showed Nur77 binding sites, and linked it with the RNA-seq dataset. The result suggested that among differentially expressed genes, there were 38 genes directly upregulated and 58 genes down-regulated by Nur77 (Figure 5C). At the same time, we found that some genes in the signal pathways with conspicuous changes were directly regulated by Nur77, such as LOX-1, FATP2, BMAL1, and Lipe. Next, we examined the mRNA expression of these genes by q-PCR. LOX-1 was most strongly affected by Nur77 deficiency (Figure 5D). Consistent with qPCR data, western blot analysis further confirmed the alteration of LOX-1 expression (Figure 5E) and celastrol restrained protein levels of LOX-1(Figure 5F). These data demonstrated that LOX-1 was upregulated by the deletion of Nur77, which could be involved in AAA.

Nur77 Suppresses LOX-1 Transcriptionally in AAA

We then tested the role of LOX-1 involved in AAA. Double immunofluorescence staining of human AAA tissues showed LOX-1 was markedly increased in AAA lesions compared to nonaneurysmal sections, and LOX-1 was expressed primarily in infiltrating macrophages (Figure 6A). Moreover, we examined the expression of LOX-1 in human AAA samples. As
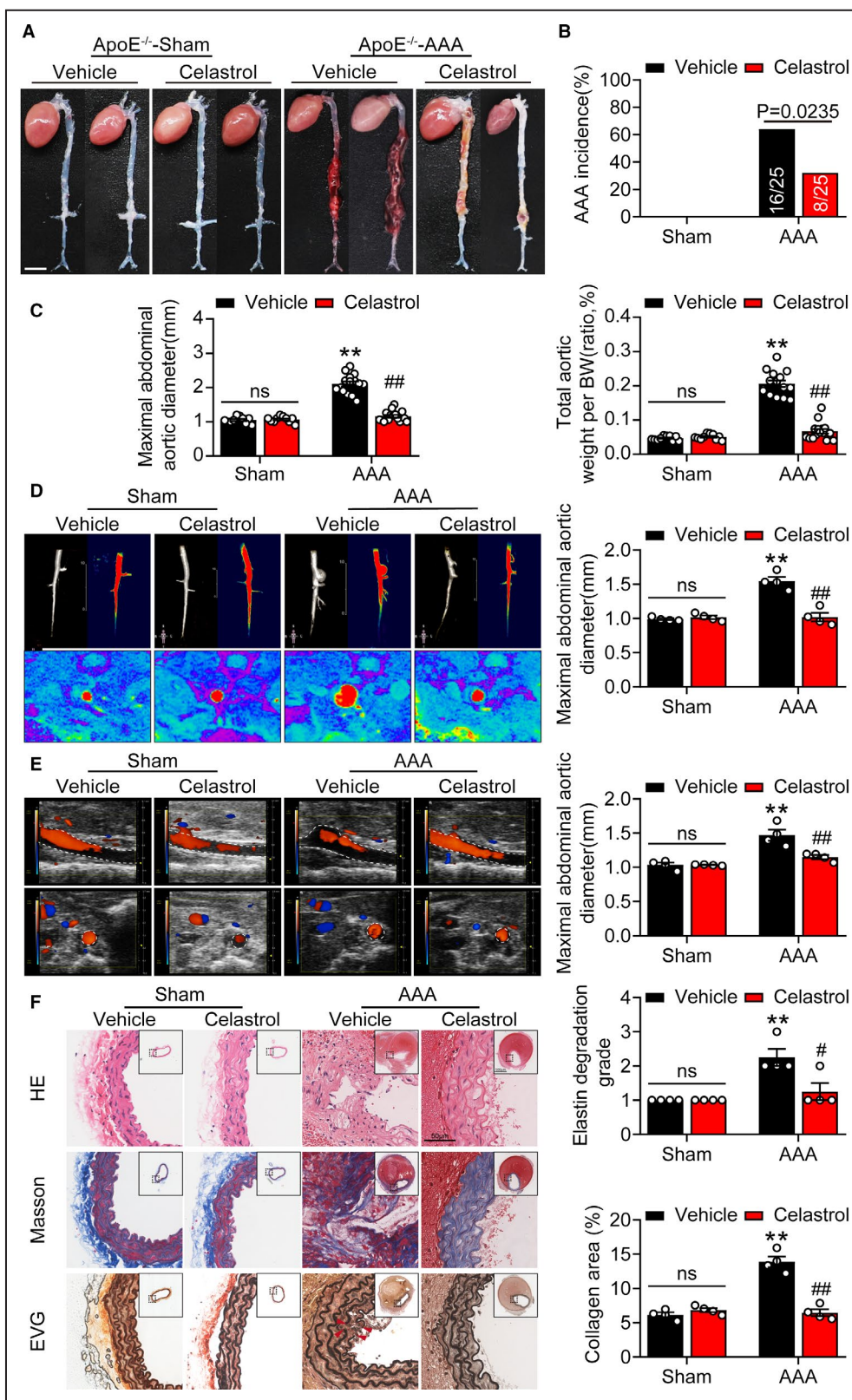
expected, LOX-1 was significantly elevated in human AAA than adjacent nonaneurysmal aortic sections (Figure 6B). These results indicated that LOX-1 might function in AAA formation.

In agreement with the in vivo results, western blot analysis confirmed the alteration of LOX-1 expression. We overexpressed or knocked down Nur77(Figure S7) and found that the protein level of LOX-1 was upregulated

Figure 3.   Nur77 agonist alleviates Ang II-induced AAA formation

A, Representative photographs showing mouse aortas treated with celastrol or vehicle after saline or Ang II infusion. Scale bar indicates 5 mm. **B**, the incidence of AAA in mice treated with celastrol or vehicle. n=10 in each group of Saline-ApoE$^{-/-}$ mice treated with vehicle or celastrol, n=25 each for Ang II-ApoE$^{-/-}$ mice treated with vehicle or celastrol. **C**, Maximal abdominal aortic diameter, total aortic weight-to-BW ratio of the indicated groups (n=10–15). **D**, Serial in vivo MRI of AAA in mice treated with celastrol or vehicle and corresponding transverse images, and the quantification of maximal abdominal aortic diameter. Red denotes 3D-reconstructed MRI images of the abdominal aorta (n=4 mice per group). **E,** Micro-ultrasound views of abdominal aortic aneurysms and the quantification of the maximal abdominal aortic diameter (n=4 mice per group). **F,** Representative images of suprarenal aortic sections stained with hematoxylin and eosin (H&E), Masson Trichrome (collagen), and Van Gieson (elastin) in mice. Right panel shows the grade of elastin degradation and collagen deposition in the aortic wall of mice (n=4 per group). ****$P<0.01$** vs vehicle-treated sham-ApoE$^{-/-}$mice; **#$P<0.05$** vs celastrol-treated AAA-ApoE$^{-/-}$mice, **##$P<0.01$** vs celastrol-treated AAA-ApoE$^{-/-}$mice. Data are presented as mean± SEM. Chi-square test for B. Two-way ANOVA followed by Tukey's multiple comparisons test for C, D, E, and F. BW, body weight; ns, nonsignificant.

in Nur77$^{-/-}$ BMDMs treated with Ang II compared to WT BMDMs. However, the upregulation of LOX-1 was abolished after celastrol treatment or Nur77 overexpression (Figure 6C). These results suggested that Nur77-deletion upregulated LOX-1 level.

To identify the mechanism by which the deletion of Nur77 upregulated LOX-1 mRNA and protein, we tested the possibility that Nur77 bound directly to the LOX-1 gene promoter and suppressed its transcription. We analyzed the mouse LOX-1 promoter DNA sequence according to the CHIP-Seq dataset, and ChIP was conducted with Ang II-treated Raw264.7 cells. ChIP assays revealed that Nur77 bound to the LOX-1 promoter, and this binding was attenuated following Ang II treatment (Figure 6D). The data above suggested that Nur77 transcriptionally inhibited LOX-1 in macrophages through directly binding to the upstream promoter of LOX-1.

Next, we performed rescue experiments in which LentiNur77-transduced Raw264.7 cells were transduced with LOX-1 plasmid to restore the expression of LOX-1 followed by Ang II treatment for 24 hours (Figure S8A, B). The results indicated that LOX-1 overexpression significantly worsened the inflammation response and increased the transcription levels of inflammatory cytokines (Figure 6E). Then the Nur77$^{-/-}$ BMDMs were transduced with siLOX-1 to downregulate LOX-1 expression (Figure S8C, D). We found that the effects of Nur77 deletion were abolished when LOX-1 was knocked down, as evidenced by decreased expression of IL-1b, TNF-α, and CCL2 (Figure 6F). Altogether, the aggravated inflammation after Nur77 knockout seemed to depend on mounting LOX-1.

DISCUSSION

The present study was the first to investigate the roles of the orphan nuclear receptor Nur77 in the pathogenesis of abdominal aortic aneurysm (AAA). Novel study findings were as follows: First, Nur77 levels were demonstrated to be downregulated in AAA lesions. Second, deletion of Nur77 aggravated the abdominal aortic aneurysms of mice induced by Ang II infusion, while pharmacological activation of Nur77 showed

beneficial effects against AAA. Third, Nur77 inhibited macrophage infiltration and reduced MMP-9 expression. Finally, mechanistic investigations revealed that Nur77 inhibited LOX-1 transcriptionally via direct binding to the promoter of LOX-1, thereby alleviating inflammatory response. Collectively, our findings suggest Nur77 could be a potential pharmacological target in AAA.

Nur77 is a nuclear receptor that functions as a transcriptional activator or repressor, and accumulating evidence indicates that Nur77 is also pivotally involved in modulating cardiovascular physiology and pathologies such as atherosclerosis,[15] cardiac hypertrophy,[21] myocardial infarction.[22] We previously reported that Nur77 reduced Ang II-induced vascular remodeling.[23] Here, we extended upon the established roles of Nur77 demonstrating that Nur77 was a negative regulator against abdominal aortic aneurysm by utilizing Nur77$^{-/-}$ mice. The current study further indicated that Nur77 activation by celastrol, a Nur77 agonist, protected against AAA. Celastrol, also known as tripterine, is a potent anti-inflammatory agent isolated from the root of *Tripterygium wilfordii*, and has been widely used in diverse indications.[24–26] Of note, it was previously demonstrated that Nur77 was a direct intracellular target of celastrol. Celastrol could bind to Nur77, which resulted in the suppression of inflammation.[27] Our studies demonstrate that celastrol treatment inhibited AAA formation, emphasizing the critical role of Nur77 in regulating AAA.

It is well recognized that macrophage activation has been strongly implicated in AAA development with contributions to inflammation and ECM remodeling.[28] Here, Nur77 deficiency was shown to exacerbate macrophage infiltration and increased inflammatory cytokines, while pharmacological activation of Nur77 counteracted these abnormalities. These observations are consistent with previous reports that Nur77 reduced inflammatory cytokine production in lesioned macrophages.[11] In addition to inflammation, matrix metalloproteinase has been recently reported as a novel regulatory target in AAA. Matrix metalloproteinases (MMPs) are a family of proteolytic enzymes that degrade various components of the extracellular
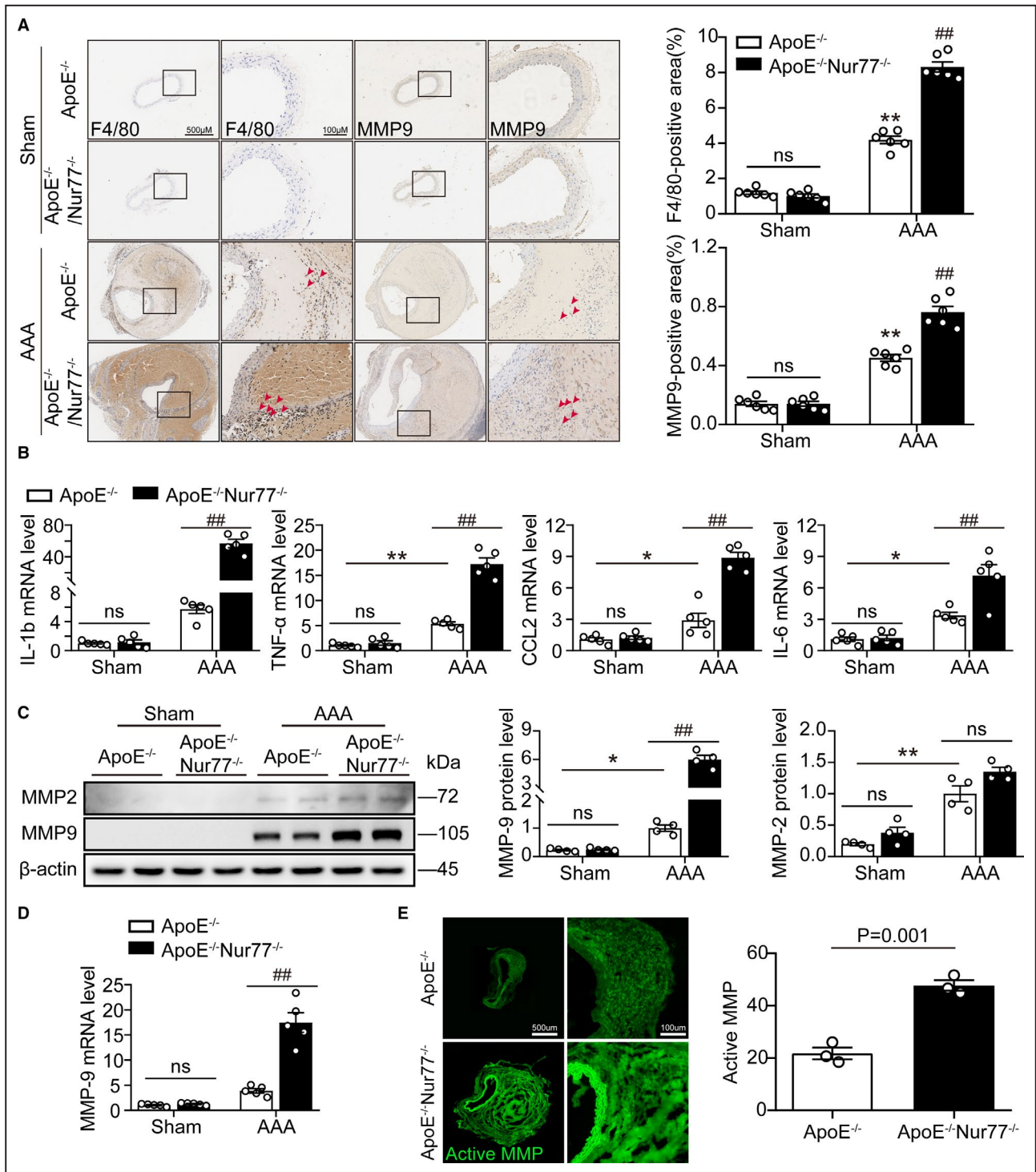
Figure 4. Nur77 deficiency enhances AAA lesion macrophage infiltration and inflammatory response

A, Representative immunohistochemical staining images showing macrophages (F4/80) and MMP-9 in mouse abdominal aortas, with the quantification results in the right panels (n=6 per group). **B,** The q-PCR analysis of inflammatory cytokines (IL-1b, TNF-α, CCL2, and IL-6) in the aortic wall (n=5 mice per group). **C,** Western blot analysis and quantitative results of MMP9 and MMP2 (n=4 mice per group). **D,** Gene expression of MMP9 in AAA lesioned tissues (n=4 mice per group). **E,** In situ zymography for gelatinase activity (n=3 per group). *$P<0.05$ vs Sham-ApoE$^{-/-}$ mice, **$P<0.01$ vs Sham-ApoE$^{-/-}$ mice; #$P<0.05$ vs AAA-ApoE$^{-/-}$ mice, ##$P<0.01$ vs AAA-ApoE$^{-/-}$ mice. Data are presented as mean ± SEM. Two-way ANOVA followed by Tukey's multiple comparisons test for A–D. Student's two-tailed t test for E. CCL2, chemokine (C-C motif) ligand 2; IL-1b, Interleukin-1β; IL-6, Interleukin-6; MMP, matrix metalloproteinase; ns, nonsignificant; TNFα, tumor necrosis factor-α.
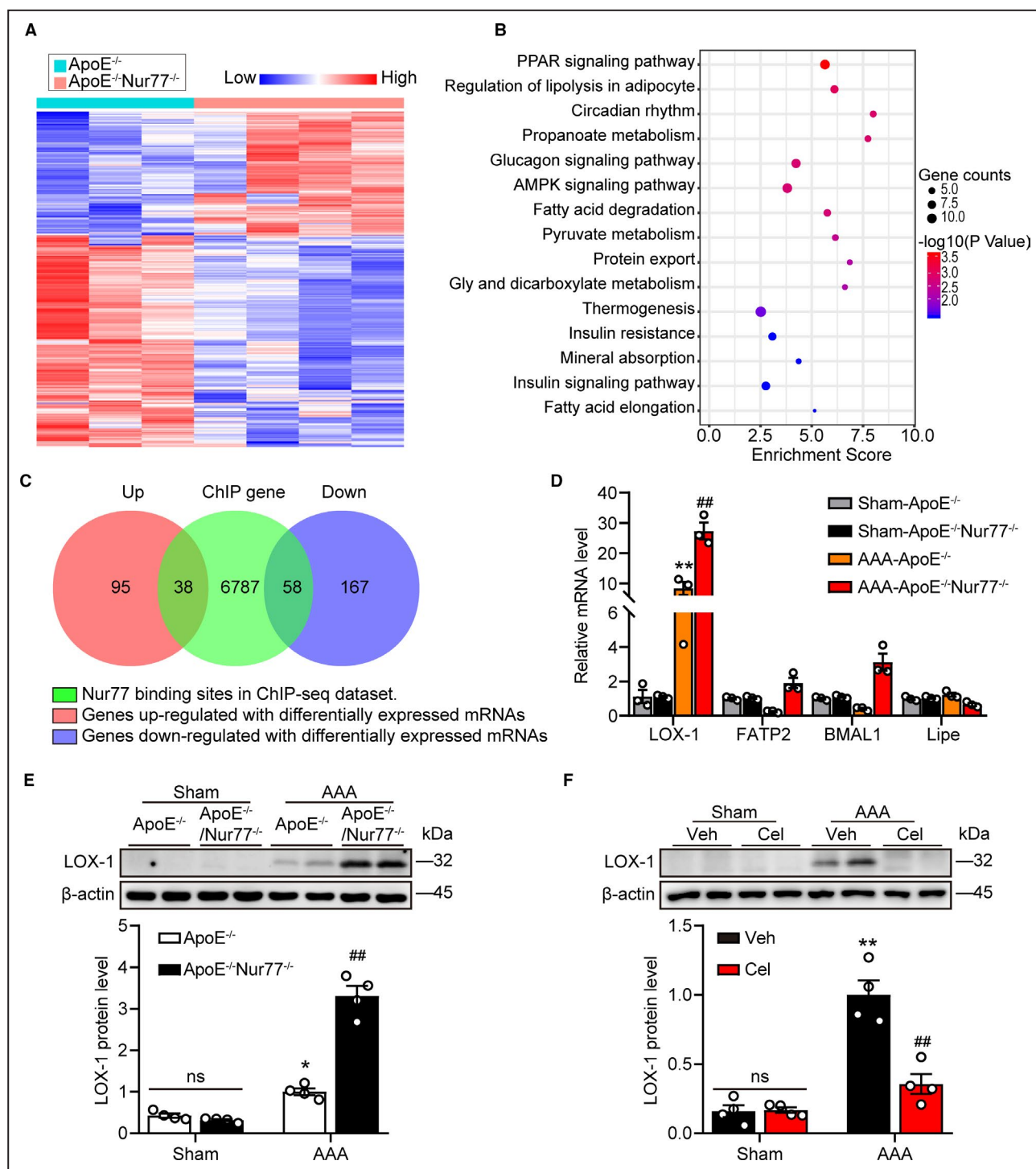
Figure 5. Nur77 deletion increases LOX-1 expression in abdominal aortas

A, Heatmap showing the differentially expressed genes between ApoE$^{-/-}$ mice and ApoE$^{-/-}$Nur77$^{-/-}$ mice with AAA (fold change ≥ 2, P<0.05). **B,** Top enriched pathways for genes in RNA-seq dataset. **C,** Venn diagram showing the overlap between Nur77 target genes in CHIP-seq dataset and differentially expressed genes in RNA-seq dataset. **D,** Transcription levels of LOX-1, Fatp2, BMAL1, and Lipe in aortas of mice were measured by q-PCR (n=3 mice per group). **E** and **F,** Western blot analysis and quantitative results of LOX-1 (n=4 mice per group). *P<0.05 vs Sham-ApoE$^{-/-}$ mice, **P<0.01 vs Sham-ApoE$^{-/-}$ mice, Sham-Veh mice; ##P<0.01 vs AAA-ApoE$^{-/-}$ mice, AAA-Veh mice. Data are presented as mean± SEM. Student's two-tailed t test for D. Two-way ANOVA followed by Tukey's multiple comparisons test for E and F. BMAL1, brain and muscle ARNT-like protein 1; Cel, celastrol; FATP2, Fatty acid transporter-2; Lipe, hormone-sensitive lipase; LOX-1, lectin like Ox-LDL receptor-1; ns, nonsignificant; Veh, vehicle;.
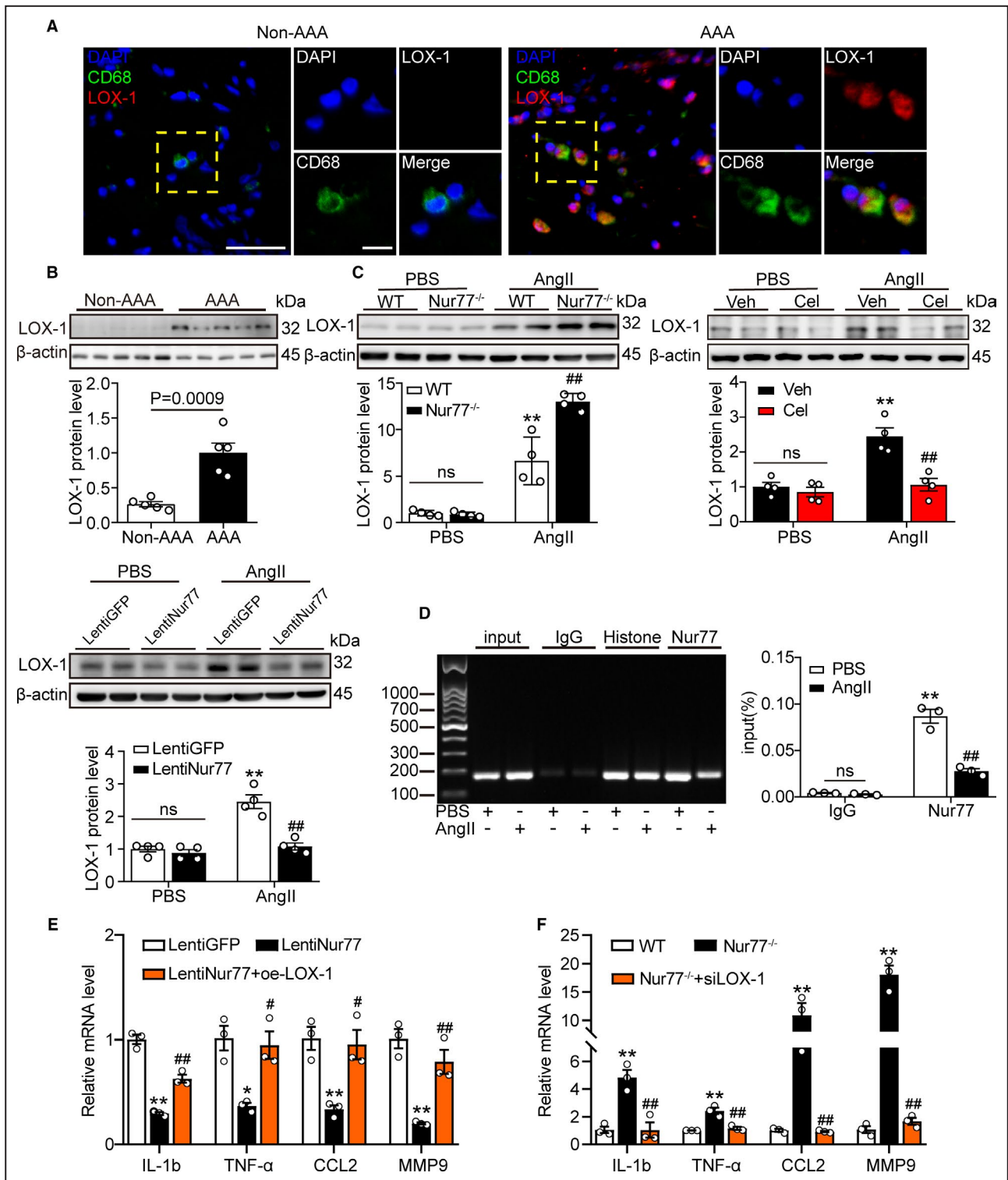
matrix (ECM). Both MMP-2 and −9 are necessary to induce experimental AAA formation in mice.[29] Previous studies reported that MMP9-knockout mice showed a suppressed mechanism of aneurysm formation.[30] Our results showed that Nur77 deletion did not affect MMP2 but significantly increased MMP9, resulting in exacerbated aneurysm development. These data provided a novel protective mechanism for Nur77 by the decrease in both inflammatory response and MMP-9 expression in the setting of AAA.

Lectin-like oxidized low-density lipoprotein receptor-1 (LOX-1) is the primary Ox-LDL receptor of endothelial cells and is also expressed in macrophages, smooth muscle cells, and platelets.[31] LOX-1 expression

**Figure 6.   Nur77 suppresses LOX-1 transcriptionally in AAA**

A, Representative photographs of double immunofluorescence staining in human AAA tissues for CD68 (green) and LOX-1 (red). Scale bar indicates 50 µm. **B**, Relative protein levels of LOX-1 in human AAA samples and adjacent control aortas (n=5 samples per group). **C**, Western blot analysis and quantitative results of LOX-1 (n=4 independent experiments per group), **$P<0.01$ vs PBS-WT, PBS-Veh or PBS-LentiGFP; ##$P<0.01$ vs Ang II-WT, Ang II-Veh or Ang II-LentiGFP. **D**, Raw264.7 cells were treated with Ang II (1 µM) for 24 h, DNA fragments from the Raw264.7 cells that contain regions of the LOX-1 promoter were immunoprecipitated with the anti-Nur77 antibody. The expression was identified by q-PCR and further confirmed by DNA gel electrophoresis (n=3 independent experiments per group, **$P<0.01$ vs PBS-IgG; ##$P<0.01$ vs PBS-Nur77). **E** and **F**, q-PCR was used to determine the transcription levels of IL-1b, TNF-α, and CCL2, MMP-9 in the indicated groups (n=3 independent experiments per group). *$P<0.05$ vs LentiGFP-Ang II, **$P <0.01$ vs LentiGFP-Ang II or WT-Ang II; #$P <0.05$ vs LentiNur77-AngII, ##$P <0.01$ vs LentiNur77-AngII or Nur77^{-/-}-Ang II. Data are presented as mean± SEM. Student's two-tailed t test for B. Two-way ANOVA followed by Tukey's multiple comparisons test for C, D. One way-ANOVA followed by Tukey's multiple comparisons test for E, F. IgG, immunoglobulin G; GFP, green fluorescent protein; Lenti, lentiviral; ns, nonsignificant; oe, overexpression; si, small interfering RNA; WT, wild type.

is low under normal physiological conditions. It is induced by inflammatory cytokines, such as tumor necrosis factor-α, IFN-γ, IL-6, and pathological conditions such as hypertension,[32,33] diabetes,[34] and atherosclerosis.[35] This property indicates that LOX-1 plays an essential role in inflammatory diseases. Furthermore, it has been found that LOX-1 gene expression is upregulated in response to Ang II,[36] but the role of LOX-1 in aortic aneurysm has not been reported. The current study provided a novel insight into this issue. We found that Nur77 bound to the LOX-1 promoter, and deletion of Nur77 resulted in increased LOX-1 mRNA and protein expression, indicating that Nur77 binds and suppresses LOX-1 transcription in AAA. Previous studies have suggested that LOX-1 was shown to activate the NF-κB signaling pathway and induce MMP-9 expression,[37,38] which may further contribute to AAA

progression. Our data suggested that LOX-1 mediated the harmful effect of Nur77 knockout in AAA.

It should be noted that Nur77 also plays diverse roles in multiple cell types. It has been previously shown that Nur77 expression was induced in vascular smooth muscle cells after Ang II stimulation.[24] Also, we have verified the expression of Nur77 in VSMC could be affected by Ang II in vivo and vitro (Figure S9). This hints at the multiple mechanisms of action of Nur77. Therefore, it remains necessary to use macrophage-specific Nur77 knockout mice to investigate the protective effects of Nur77 in macrophage against AAA.

In summary, the results of this study demonstrate an essential role of Nur77 in Ang II infusion-induced experimental AAA in mice, and the details are described in Figure 7. Our findings may provide a promising therapeutic target for the treatment of AAA.
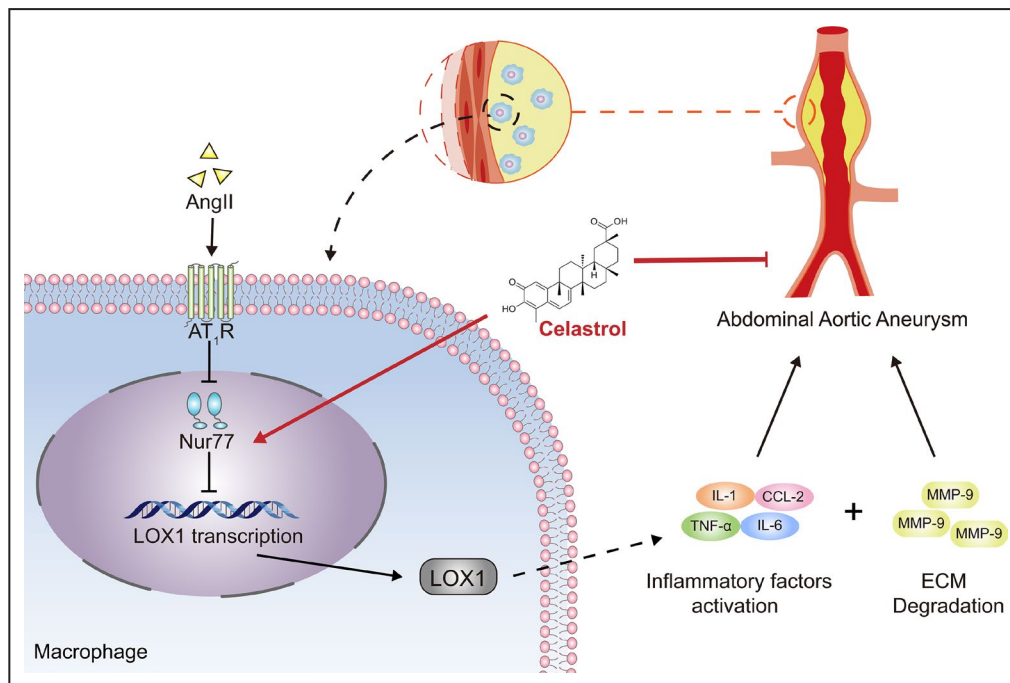
Figure 7.   Protective functions of Nur77 in abdominal aortic aneurysm

In mice, Nur77 reduces AAA incidence and suppresses the progression of AAA, which is associated with alleviated inflammatory response and matrix metalloproteinase expression. LOX-1 mediated the protective role of Nur77 in these processes.

REFERENCES

1. Golledge J, Kuivaniemi H. Genetics of abdominal aortic aneurysm. *Curr Opin Cardiol*. 2013;28:290–296. DOI: 10.1097/HCO.0b013e32835f0d55.

2. Golledge J, Norman PE. Current status of medical management for abdominal aortic aneurysm. *Atherosclerosis*. 2011;217:57–63. DOI: 10.1016/j.atherosclerosis.2011.03.006.

3. Raffort J, Lareyre F, Clément M, Hassen-Khodja R, Chinetti G, Mallat Z. Monocytes and macrophages in abdominal aortic aneurysm. *Nat Rev Cardiol*. 2017;14:457–471.

4. Li H, Bai S, Ao Q, Wang X, Tian X, Li X, Tong H, Hou W, Fan J. Modulation of immune-inflammatory responses in abdominal aortic aneurysm: Emerging molecular targets. *Journal of Immunology research*. 2018;2018:7213760. DOI: 10.1155/2018/7213760.

5. Murray PJ, Wynn TA. Protective and pathogenic functions of macrophage subsets. *Nat Rev Immunol*. 2011;11:723–737.

6. Hadi T, Boytard L, Silvestro M, Alebrahim D, Jacob S, Feinstein J, Barone K, Spiro W, Hutchison S, Simon R, et al. Macrophage-derived netrin-1 promotes abdominal aortic aneurysm formation by activating mmp3 in vascular smooth muscle cells. *Nat Commun*. 2018;9:5022. DOI: 10.1038/s41467-018-07495-1.

7. Tazume H, Miyata K, Tian Z, Endo M, Horiguchi H, Takahashi O, Horio E, Tsukano H, Kadomatsu T, Nakashima Y, et al. Macrophage-derived angiopoietin-like protein 2 accelerates development of abdominal aortic aneurysm. *Arterioscler Thromb Vasc Biol*. 2012;32:1400–1409. DOI: 10.1161/ATVBAHA.112.247866.

8. McCormick ML, Gavrila D, Weintraub NL. Role of oxidative stress in the pathogenesis of abdominal aortic aneurysms. *Arterioscler Thromb Vasc Biol*. 2007;27:461–469. DOI: 10.1161/01.ATV.0000257552.94483.14.

9. Hamers AA, Hanna RN, Nowyhed H, Hedrick CC, de Vries CJ. Nr4a nuclear receptors in immunity and atherosclerosis. *Curr Opin Lipidol*. 2013;24:381–385. DOI: 10.1097/MOL.0b013e3283643eac.

10. McMorrow JP, Murphy EP. Inflammation: a role for nr4a orphan nuclear receptors? *Biochem Soc Trans*. 2011;39:688–693. DOI: 10.1042/BST0390688.

11. Bonta PI, van Tiel CM, Vos M, Pols TWH, van Thienen JV, Ferreira V, Arkenbout EK, Seppen J, Spek CA, van der Poll T, et al. Nuclear receptors nur77, nurr1, and nor-1 expressed in atherosclerotic lesion macrophages reduce lipid loading and inflammatory responses. *Arterioscler Thromb Vasc Biol*. 2006;26:2288–2294. DOI: 10.1161/01.ATV.0000238346.84458.5d.

12. Pei L, Castrillo A, Chen M, Hoffmann A, Tontonoz P. Induction of nr4a orphan nuclear receptor expression in macrophages in response to inflammatory stimuli. *The Journal of biological chemistry*. 2005;280:29256–29262. DOI: 10.1074/jbc.M502606200.

13. Shao Q, Han F, Peng S, He B. Nur77 inhibits oxldl induced apoptosis of macrophages via the p38 mapk signaling pathway. *Biochem Biophys Res Commun*. 2016;471:633–638. DOI: 10.1016/j.bbrc.2016.01.004.

14. Shao Q, Shen LH, Hu LH, Pu J, Qi MY, Li WQ, Tian FJ, Jing Q, He B. Nuclear receptor nur77 suppresses inflammatory response dependent on cox-2 in macrophages induced by oxldl. *J Mol Cell Cardiol*. 2010;49:304–311. DOI: 10.1016/j.yjmcc.2010.03.023.

15. Hanna RN, Shaked I, Hubbeling HG, Punt JA, Wu R, Herrley E, Zaugg C, Pei H, Geissmann F, Ley K, et al. Nr4a1 (nur77) deletion polarizes macrophages toward an inflammatory phenotype and increases atherosclerosis. *Circ Res*. 2012;110:416–427. DOI: 10.1161/CIRCRESAHA.111.253377.

16. Cheng Z, Völkers M, Din S, Avitabile D, Khan M, Gude N, Mohsin S, Bo T, Truffa S, Alvarez R, et al. Mitochondrial translocation of nur77 mediates cardiomyocyte apoptosis. *Eur Heart J*. 2011;32:2179–2188. DOI: 10.1093/eurheartj/ehq496.

17. Wang R-H, He J-P, Su M-L, Luo J, Xu M, Du X-D, Chen H-Z, Wang W-J, Wang Y, Zhang N, et al. The orphan receptor tr3 participates in angiotensin ii-induced cardiac hypertrophy by controlling mtor signalling. *EMBO Mol Med*. 2013;5:137–148. DOI: 10.1002/emmm.201201369.

18. Daugherty A, Manning MW, Cassis LA. Angiotensin ii promotes atherosclerotic lesions and aneurysms in apolipoprotein e-deficient mice. *J Clin Investig*. 2000;105:1605–1612. DOI: 10.1172/JCI7818.

19. Zhang L, Wang Q, Liu W, Liu F, Ji A, Li Y. The orphan nuclear receptor 4a1: A potential new therapeutic target for metabolic diseases. *Journal of Diabetes Research*. 2018;2018:9363461. DOI: 10.1155/2018/9363461.

20. Tang M, Cao X, Zhang K, Li Y, Zheng QY, Li GQ, He QH, Li SJ, Xu GL, Zhang KQ. Celastrol alleviates renal fibrosis by upregulating cannabinoid receptor 2 expression. *Cell Death Dis*. 2018;9:601. DOI: 10.1038/s41419-018-0666-y.

21. Medzikovic L, van Roomen C, Baartscheer A, van Loenen PB, de Vos J, Bakker ENTP, Koenis DS, Damanafshan A, Creemers EE, Arkenbout EK, et al. Nur77 protects against adverse cardiac remodelling by limiting neuropeptide y signalling in the sympathoadrenal-cardiac axis. *Cardiovasc Res*. 2018;114:1617–1628. DOI: 10.1093/cvr/cvy125.

22. Hilgendorf I, Gerhardt LM, Tan TC, Winter C, Holderried TA, Chousterman BG, Iwamoto Y, Liao R, Zirlik A, Scherer-Crosbie M, et al. Ly-6chigh monocytes depend on nr4a1 to balance both inflammatory and reparative phases in the infarcted myocardium. *Circ Res*. 2014;114:1611–1622.

23. Cui M, Cai Z, Chu S, Sun Z, Wang X, Hu L, Yi J, Shen L, He B. Orphan nuclear receptor nur77 inhibits angiotensin ii-induced vascular remodeling via downregulation of β-catenin. *Hypertension (Dallas, Tex. 1979)*;2016;67:153–162.

24. Allison AC, Cacabelos R, Lombardi VR, Alvarez XA, Vigo C. Celastrol, a potent antioxidant and anti-inflammatory drug, as a possible treatment for alzheimer's disease. *Prog Neuropsychopharmacol Biol Psychiatry*. 2001;25:1341–1357. DOI: 10.1016/S0278-5846(01)00192-0.

25. Luo D, Guo Y, Cheng Y, Zhao J, Wang Y, Rong J. Natural product celastrol suppressed macrophage m1 polarization against inflammation in diet-induced obese mice via regulating nrf2/ho-1, map kinase and nf-κb pathways. *Aging*. 2017;9:2069–2082. DOI: 10.18632/aging.101302.

26. Tao X, Younger J, Fan FZ, Wang B, Lipsky PE. Benefit of an extract of tripterygium wilfordii hook f in patients with rheumatoid arthritis: A double-blind, placebo-controlled study. *Arthritis Rheum*. 2002;46:1735–1743. DOI: 10.1002/art.10411.

27. Hu M, Luo Q, Alitongbieke G, Chong S, Xu C, Xie L, Chen X, Zhang D, Zhou Y, Wang Z, et al. Celastrol-induced nur77 interaction with traf2 alleviates inflammation by promoting mitochondrial ubiquitination and autophagy. *Mol Cell*. 2017;66:141–153.e146. DOI: 10.1016/j.molcel.2017.03.008.

28. Davis FM, Rateri DL, Daugherty A. Mechanisms of aortic aneurysm formation: translating preclinical studies into clinical therapies. *Heart (British Cardiac Society)*. 2014;100:1498–1505. DOI: 10.1136/heartjnl-2014-305648.

29. Longo GM, Xiong W, Greiner TC, Zhao Y, Fiotti N, Baxter BT. Matrix metalloproteinases 2 and 9 work in concert to produce aortic aneurysms. *J Clin Investig*. 2002;110:625–632. DOI: 10.1172/JCI0215334.

30. Pyo R, Lee JK, Shipley JM, Curci JA, Mao D, Ziporin SJ, Ennis TL, Shapiro SD, Senior RM, Thompson RW. Targeted gene disruption of matrix metalloproteinase-9 (gelatinase b) suppresses development of experimental abdominal aortic aneurysms. *J Clin Investig*. 2000;105:1641–1649. DOI: 10.1172/JCI8931.

31. Pirillo A, Norata GD, Catapano AL. Lox-1, oxldl, and atherosclerosis. *Mediators Inflamm*. 2013;2013:1–12. DOI: 10.1155/2013/152786.

32. Chen M, Kakutani M, Minami M, Kataoka H, Kume N, Narumiya S, Kita T, Masaki T, Sawamura T. Increased expression of lectin-like oxidized

low density lipoprotein receptor-1 in initial atherosclerotic lesions of watanabe heritable hyperlipidemic rabbits. *Arterioscler Thromb Vasc Biol.* 2000;20:1107–1115. DOI: 10.1161/01.ATV.20.4.1107.

33. Nagase M, Hirose S, Sawamura T, Masaki T, Fujita T. Enhanced expression of endothelial oxidized low-density lipoprotein receptor (lox-1) in hypertensive rats. *Biochem Biophys Res Comm.* 1997;237:496–498. DOI: 10.1006/bbrc.1997.7176.

34. Chen M, Nagase M, Fujita T, Narumiya S, Masaki T, Sawamura T. Diabetes enhances lectin-like oxidized ldl receptor-1 (lox-1) expression in the vascular endothelium: Possible role of lox-1 ligand and age. *Biochem Biophys Res Comm.* 2001;287:962–968. DOI: 10.1006/bbrc.2001.5674.

35. Mehta JL, Sanada N, Hu CP, Chen J, Dandapat A, Sugawara F, Satoh H, Inoue K, Kawase Y, Jishage K-I, et al. Deletion of lox-1 reduces atherogenesis in ldlr knockout mice fed high cholesterol diet. *Circ Res.* 2007;100:1634–1642. DOI: 10.1161/CIRCRESAHA.107.149724.

36. Chen J, Liu Y, Liu H, Hermonat PL, Mehta JL. Molecular dissection of angiotensin ii-activated human lox-1 promoter. *Arterioscler Thromb Vasc Biol.* 2006;26:1163–1168. DOI: 10.1161/01.ATV.0000209998. 73303.b5.

37. Li L, Renier G. The oral anti-diabetic agent, gliclazide, inhibits oxidized ldl-mediated lox-1 expression, metalloproteinase-9 secretion and apoptosis in human aortic endothelial cells. *Atherosclerosis.* 2009;204:40–46. DOI: 10.1016/j.atherosclerosis.2008.08.008.

38. Xu S, Ogura S, Chen J, Little PJ, Moss J, Liu P. Lox-1 in atherosclerosis: Biological functions and pharmacological modifiers. *Cellular and molecular life sciences: CMLS.* 2013;70:2859–2872. DOI: 10.1007/s0001 8-012-1194-z.

39. Satoh K, Nigro P, Matoba T, O'Dell MR, Cui Z, Shi XI, Mohan A, Yan C, Abe J-I, Illig KA, et al. Cyclophilin a enhances vascular oxidative stress and the development of angiotensin ii-induced aortic aneurysms. *Nat Med.* 2009;15:649–656. DOI: 10.1038/nm.1958.

40. Wang Y, Chen C, Wang Q, Cao Y, Xu L, Qi R. Inhibitory effects of cyclo-astragenol on abdominal aortic aneurysm and its related mechanisms. *Br J Pharmacol.* 2019;176:282–296. DOI: 10.1111/bph.14515.

SUPPLEMENTAL MATERIAL

Data S1.

Supplemental Methods

Human aortic samples

Human AAA tissue was obtained from 5 patients undergoing open AAA repair, and the control samples were trimmed from the nondilating aorta surrounding the lesions from the same patients. Written informed consent was obtained from all subjects before participation. All the studies involving human samples were approved by the Ethics Committee of Ren Ji Hospital (KY2020-151), School of Medicine, Shanghai Jiao Tong University, and conformed to the principles outlined in the Declaration of Helsinki.

Nur77$^{-/-}$ mice construction

CRISPR/Cas9 technology was used to introduce the mutation by non-homologous end joining (NHEJ), resulting in a frameshift of the Nur77 protein reading frame and loss of function. The brief process is as follows: The transcript of Nur77 was obtained from the Ensemble database(ENSMUST00000023779.7). The gRNAs were constructed through the website (http://crispr.mit.edu/), and gRNAs with the highest score were selected (The sequence is provided in Table S2). Then Cas9 mRNA and gRNAs were obtained by vitro transcription. Cas9 mRNA and gRNAs were microinjected into the fertilized eggs of C57BL/6J mice. The injected fertilized eggs were transplanted into pseudo-pregnant female mice, and the born mice were F0 generation mice. Since the early cleavage rate of fertilized eggs is very fast, the F0 generation mice obtained were chimeras and may not have the ability to stabilize heredity. The F0 generation mice identified by PCR (primer information is provided in Table S2) were mated with wild-type C57BL/6J mice to obtain F1 generation heterozygous mice (Nur77$^{+/-}$). Nur77$^{+/-}$ mice were

inbred to obtain Nur77$^{-/-}$ mice. The baseline date of Nur77$^{-/-}$ mice is presented in Figure S1.

Blood Pressure Measurement

The blood pressure was measured by a noninvasive blood pressure system for mice (BP-2010A, Softron Biotechnology). Briefly, mice's blood pressure was measured by putting the mice tail into the tail-cuff system in a dark quiet room and waiting for the mice to calm down to read the meter. The measurements were carried out in conscious mice without anesthesia. To avoid variations in blood pressure due to day cycle, all measurements were performed between 2 and 6 pm. Systolic blood pressure values were derived from an average of five measurements per animal.

Tissue collection

After 4 weeks, mice were euthanized with an inhalation overdose of isoflurane (3%). Then, left cardiac ventricles were immediately perfused with ice-cold isotonic saline (10ml) with an exit through the severed right atrium. After aortic tissues were isolated, the aorta's morphology was photographed. And the maximum diameters of the abdominal aortas were measured using calipers. An aneurysm was defined as a >50% increase in suprarenal aorta diameter compared with aortas from saline-infused mice. Then the abdominal aortic was dissected into two sections. One section was stored at -80°C for molecular analysis and the other section was fixed overnight in 10% formalin and then embedded in paraffin or optimal cutting temperature (OCT) embedding compound (Tissue-Tek). Serial sections (8-10 mm) of the aortas were prepared for morphometric analysis and immunofluorescence staining.

Histomorphology analysis

After the serial 8μm sections were cut, the paraffin-embedded abdominal aorta sections were stained with hematoxylin and eosin for general morphology, Masson's Trichrome for fibrosis detection, or Verhoeff-van Gieson staining (EVG) for elastin. Serial sections of aneurysm were processed with hematoxylin and eosin staining. Section levels with lesions severity ranked among the top

three were chosen to undergo further histomorphology analysis and immunohistochemistry processes to acquire the averages of indicated parameters. All samples were processed with the same protocol. Images were captured under the identical microscope (Leica DM3000B, Germany), and were analyzed using Image-Pro Plus 6.0 (Media Cybernetics Inc). Determination of elastin degradation was performed by semiquantitative grading as described previously[39]. The grades were defined as follows: grade 1, no degradation; grade 2, mild elastin degradation; grade 3, severe elastin degradation; and grade 4, aortic rupture.

Immunohistochemistry staining of F4/80 and MMP9 was used to observe the macrophage infiltration, as well as expression of MMP9 in the mice aorta, as previously described[40]. In brief, primary antibody against F4/80 (1:200) or MMP-9 (1:200) were used. Specific labeling was detected with an HRP-conjugated goat anti-rabbit secondary antibody (1:200), and then were incubated with DAB substrate (cat#ab64238, Abcam) for 10 min. Representative images were captured by light microscopy.

Immunofluorescence staining

Frozen sections were fixed by 4% paraformaldehyde for 15 min and permeabilized in cold methanol for 10min at room temperature. After blocking with 5% BSA for 1h, the sections were incubated with primary antibodies against Nur77(1:200), CD68(1:200), LOX-1(1:200), overnight at 4°C, followed by incubation with Secondary antibodies, an Alexa Fluor 488 goat anti-mouse secondary antibody (1:200) or an Alexa Fluor 555 goat anti-rabbit secondary antibody (1:200), for 1h at room temperature. DAPI (S36973, Thermo Scientific) was used to identify nuclei. The stained sections were viewed using fluorescence microscopy.

In situ MMP zymography

In situ MMP zymography was performed using Gelatinase Assay Kit following the manufacturer's instruction (GMS80062.1, Genmed Scientifics Inc). In brief, abdominal aortas were OCT embedded and freshly cut into 8 μm

sections using a freezing microtome. Gelatinolytic activity was analyzed in unfixed frozen sections using FITC-labeled gelatin as a substrate. Slides were incubated at room temperature, protected from light for 2h. Proteolytic activity was detected as green fluorescence (530 nm) by fluorescence microscopy (Leica DM3000B, Germany).

Cell culture and treatment

Ang II was used to induce AAA in vitro model. Raw264.7 cells (murine macrophage cell line) and Movas (mouse aorta smooth muscle cell line) from the Cell Bank of the Chinese Academy of Sciences (Shanghai, China) were cultured in Dulbecco's Modified Eagle's Medium (DMEM, Gibco) supplemented with 10% fetal bovine serum (FBS, Gibco), 100U/mL of penicillin and 100μg/mL of streptomycin at 37°C in a humidified 5% CO_2 atmosphere. Cells were collected after incubating with Ang II (1μmol/L) for the selected time (0, 0.5, 1, 3, 6,12h). In a separate experiment, the Cells were pretreated with or without celastrol (0.3μM) for 2h, followed by treatment with Ang II (1μmol/L) for 12h. Cells were treated with serum-free DMEM for 12h before drug treatment.

Bone marrow-derived macrophage (BMDM) isolation and culture

Bone marrow cells were prepared from femurs and tibiae of 6- to 8-week-old WT and Nur77^{-/-}mice as previously described[15]. Briefly, mice were euthanized with an inhalation overdose of isoflurane (3%). Next, surgically removed cleaned bones were transferred into a sterile Petri dish containing ice-cold, sterile 1x PBS (10 ml), and the marrow was flushed with PBS in a syringe with a 27-gauge needle. Simultaneously, the needle was moved up and down while scraping the inside of the bone to dissociate the cells until the bone appears clear. Cell suspension was centrifuged at 150g for 5 minutes at 4°C. The supernatant was discarded and the cells were resuspended and seeded in 6-well plates with complete DMEM containing 10% FBS, 2 mM glutamine, 100 U/ml penicillin, 100μg/ml streptomycin, and supplement with 30 ng/ml recombinant M-CSF (416-ML-050, R&D Systems). The plate was Incubate at 37 °C and 5% CO_2. Fresh BMDM growth medium was changed on day 3. On

day 7, the mature BMDM can be used for subsequent experiments.

Lentiviral transduction, LOX-1 overexpression and knockdown

To overexpress Nur77, lentivirus was purchased from Genomeditech Co, Ltd. (Shanghai, China) and stable cell lines were constructed by the lentivirus infection. A similar lentiviral vector encoding the green fluorescent protein (GFP) gene (LentiGFP) was used as a control. Raw264.7 cells were transduced with lentiviral in diluted media at a multiplicity of transduction of 100 for 48h and then cultured in DMEM media containing 10% bovine serum.

To overexpress and knockdown LOX-1. Plasmids including overexpression negative control plasmid (oe-NC), LOX-1 overexpression plasmid (oe-LOX-1), small interfering RNA targeting LOX-1 (si-LOX-1), and si-NC were all purchased from Shanghai Genomeditech (Shanghai, China). Cells in 6-well plates were transfected with plasmid or siRNA using Lipofectamine™3000 (L3000150, Invitrogen) according to the manufacturer's instructions. After transfection for 24h, the mRNA and protein expression of the cells were detected, respectively.

MRI screening assay

Magnetic resonance imaging (MRI) was performed at weeks 4 after surgery. All scanning was carried out with a 7.0-T small animal, Superconducting magnet and BioSpec spectrometer (BioSpec 70/20 USR: Bruker, Bruker Biospin, Ettlingen, Germany). All mice were induced and maintained under isoflurane anesthesia (1.5% to 2%) in medical-grade and monitored simultaneously via a sensor positioned on the abdomen for respiration rate (30-50 breath/min). All MRI images were acquired according to the manufacturer's instruction. RadiAnt DICOM Viewer (Poznan, Poland) software was used to delineate an ROI to determine the abdominal aorta cross-sectional area.

Vascular ultrasound imaging

Micro-ultrasound images were obtained using the Vevo770 system (Visual Sonics) 4 weeks after surgery. Mice were anesthetized using 1.5%-2.0% isoflurane, the abdominal hair was removed using depilatory cream and

ultrasound transmission gel was added onto the abdomen area to acquire optimal images. Heart rate and respiration were monitored throughout the procedure. An ultrasonic probe was first applied on the transverse plane to locate the abdominal aorta, the "Portal Triad" (hepatic artery, hepatic vein, and bile duct) was used as anatomic markers to confirm the location of the aorta. The aorta was centered and the probe was moved down to find the kidney. Color mode Doppler was activated to help localize the two renal arteries, and the probe then switched to the long axis. The probe was placed parallel to the aorta to obtain a longitudinal axis view of the abdominal aorta. Images were recorded to acquire measurements of the aortic diameter.

Quantitative real-time PCR

Total RNA was extracted from AAA and sham control tissues or cells using RNAiso Plus (Takara). cDNA was synthesized using PrimeScript RT Master Mix kit (Takara). qRT-PCR of mRNAs was performed using TB Green® Premix Ex Taq™ (Takara) and real-time PCR experiments were carried on a LightCycler® 480 System (Roche). Quantitative results were normalized against GAPDH and presented by the $2^{-\Delta Ct}$ method. The primers used for q-PCR are listed in Table S3.

Western blot analysis

Total proteins were extracted from cells or from abdominal aortas of the mice and lysed in lysis buffer (Roche, USA) with the protease and phosphatase inhibitor (Thermo Scientific) for 30 min on the ice. The supernatant fluid was then collected after centrifugation. Proteins were separated by 7%-12.5% SDS-PAGE gels and transferred onto PVDF membranes (Millipore, Bedford, MA). Membranes were blocked with 5% non-fat dry milk in TBST for 1h at room temperature and incubated overnight at 4°C with different primary antibodies. Membranes were washed and incubated with horseradish peroxidase-conjugated anti-rabbit IgG (cat#111-035-003, Jackson ImmunoResearch) for 1h at room temperature. GAPDH, β-actin, or tubulin acted as the control. Protein bands were detected with LAS-4000 mini system (Fujifilm, Japan).

Chromatin immunoprecipitation (ChIP) analysis

ChIP assay was performed with SimpleChIP® Enzymatic Chromatin IP Kit (Cat#9003, Cell Signaling Technology) according to manufacturer's instructions. Raw 264.7 cells were treated with PBS or Ang II (1μmol/L) for 12h. Crosslinking of chromatin was performed by treatment with 1% formaldehyde for exactly 10 minutes at room temperature. Then, glycine was added into the culture medium to terminate the crosslinking reaction. After termination of crosslinking, nuclear extraction from cell pellets was performed with SimpleChIP® Enzymatic Chromatin IP Kit. Crosslinked chromatin was sheared to 150-900 bp with micrococcal nuclease. Then the lysate was treated with 3 sets of 20-sec pulse using an Ultrasonic Sonicator. Immunoprecipitation was performed with 2μg anti-IgG antibody (CST) and 10ul anti-Histone H3 Rabbit antibody (CST) as negative and positive control of ChIP, respectively. As a target antibody, 10μg polyclonal anti-Nur77 antibody was used. ChIP PCR was performed with primers encompassing the following loci of the LOX-1 promoter in mice: forward:5′-TGGACTGGATGGTTCGACTTG-3′ reverse:5′-ACTCAGGGCCAGGAATGGAA-3′. Then LOX-1 promoter-specific PCR products were subjected to agarose gel electrophoresis analysis.

RNA sequencing

Total RNA was extracted using the mirVana miRNA Isolation Kit (Ambion) following the manufacturer's protocol. RNA quality was verified using the Agilent 2100 Bioanalyzer (Agilent Technologies, Santa Clara, CA, USA). Then the libraries were constructed using TruSeq Stranded mRNA LT Sample Prep Kit (Illumina, San Diego, CA, USA) according to the manufacturer's instructions. Then, these libraries were sequenced on the Illumina sequencing platform (Illumina HiSeq X Ten) and 125 bp/150 bp paired-end reads were generated. Differentially expressed genes (DEGs) were identified using the DESeq R package functions to estimate Size Factors and nbinomTest. P-value < 0.05 and foldchange>2 or foldchange<0.5 was set as the threshold for significantly differential expression. KEGG pathway enrichment analysis of DEGs was

performed respectively using R based on the hypergeometric distribution. RNA-Seq Data had been submitted to GEO(GSE174768). Principal component analysis (PCA) is presented in Figure S4. QC metrics for the RNA-seq data are shown in Table S4.

ChIP-Sequencing analysis

The data downloaded from the GEO database (GSE102393) were, respectively, SRR5914767.1, SRR988407.2, SRR988408.2, SRR1694053.1. The quality control of clean data was performed by FastQC. All reads were mapped to the mm10 mouse genome using bwa program, and uniquely mapped reads were processed further for peak identification. MACS14 was used to identify significant peaks with input DNA (ChIP–seq) as the control, and -p 10^{-7} was used as the threshold for peak calibration. Then R package ChIPseeker was used to annotate the peak identification results. The consensus binding motif analysis for Nur77 was performed by MEME.

Supplemental statistical analysis

Blinding was used in the study. According to our randomization and blinding strategy, animals were grouped by Dr. Che, and the surgery was operated by Dr. Zhang. The color Doppler ultrasound and MRI scans were carried out by Dr. Geng. Slide scoring and follow-up study were performed by Dr. Sun, assisted by Dr. Chen. The researchers except Dr. Che were unaware of the treatment group assignment or genotype.

Table S1. Key Resource Table.

Regents or Resources	Source	Identity
Angiotensin-II	Sigma-Aldrich	A9525
Celastrol	MedChemExpress	HY-13067
Isoflurane	RWD	R510-22
OCT embedding compound	Sakura	4583
H&E kit	Servicebio	G1005-500ML
Masson's Trichrome kit	Servicebio	G1006-100ML
EVG dye solution set	Servicebio	G1042
DAPI	Thermo Scientific	S36973
Gelatinase Assay Kit	Genmed Scientifics	GMS80062.1
DMEM	Gibco	10569-010
Fetal bovine serum	Gibco	10099-141
M-CSF	R&D Systems	416-ML-050
Cell Counting Kit-8 assay	Beyotime	C0041
Lipofectamine™3000	Invitrogen	L3000150
RNAiso Plus	Takara	9108
PrimeScript RT Master Mix kit	Takara	RR036A
TB Green® Premix Ex Taq™	Takara	RR420A
Complete lysis-M	Roche	04719964001
Protease and phosphatase inhibitor	Thermo Scientific	78443
SimpleChIP®Enzymatic Chromatin IP Kit	Cell Signaling Technology	9003
Osmotic Pumps	Alzet	2004
DAB substrate	Abcam	ab64238
Mouse anti-CD68	Abcam	ab31630
Mouse anti-CD68	Abcam	ab955
Rabbit anti-Nur77	Abcam	ab13851

Mouse anti-alpha smooth muscle Actin	Abcam	Ab7817
Rabbit anti-LOX-1	Abcam	ab60178
Rabbit anti-GAPDH	Abcam	ab371668
Rabbit anti-β-actin	Cell Signaling Technology	4970
Rabbit anti-MMP-2	Abcam	ab37150
Rabbit anti-MMP-9	Abcam	ab38898
Rabbit anti-F4/80	Abcam	ab111101
Goat anti-rabbit (HRP)	Jackson ImmunoResearch	111-035-003
Alexa Fluor 488 goat anti-Mouse	Cell Signaling Technology	A-11001
Alexa Fluor 555 goat anti-Rabbit	Cell Signaling Technology	A-21428
Goat Anti-Rabbit IgG H&L (HRP polymer)	Abcam	ab214880
Raw264.7 cell	Cell Bank of the Chinese Academy of Sciences (Shanghai, China)	
Movas cell	Cell Bank of the Chinese Academy of Sciences (Shanghai, China)	
ApoE$^{-/-}$ mice on a C57BL/6 background	Shanghai Model Organisms Center	NM-KO-190565
C57BL/6 mice	Beijing SPF Biotechnology Co., Ltd.	SPF-A04-001

Table S2. gRNAs sequence.

gRNAs	Sequence (5'-3')
gRNA1	CCTTCCTCTACCAGCTGCCGGGG
gRNA2	ACCAGCCACCCACCAGCTTGGGG

Primer information

Primer Type	Sequence (5'-3')
Forward	CCCTCCCCGGCCTACCAAGTT
Reverse	TGTGCCCTGCTGAATAAAAGTCC

The primer information for F0 generation mice identification

Supplemental Table S3

PCR production	Oligoes for mutations (forward/reverse)
Human GAPDH	**5'-ACAACTTTGGTATCGTGGAAGG-3'**
	5'-GCCATCACGCCACAGTTTC-3'
Human Nur77	**5'-TGGCTGAGGACGAGGATGTGG-3'**
	5'-GCACCTTCATGGACGGCTACAC-3'
Mouse GAPDH	5'-AGGTCGGTGTGAACGGATTTG-3'
	5'-TGTAGACCATGTAGTTGAGGTCA-3'
Mouse Nur77	5'-TGTCCGCTCTGGTCCTCATCAC-3'
	5'-TCTCCTGCCACGGTAGCCATG-3'
Mouse MMP9	5'-CGCCACCACAGCCAACTATGAC-3'
	5'-CTGCTTGCCCAGGAAGACGAAG-3'
Mouse IL-1β	5'-GATGGCTGCACTATTCCTAATGCC-3'
	5'-ATGGCTCTGAGAGACCTGACTTG-3'
Mouse TNF-α	5'-TCCCAGGTTCTCTTCAAGGGA-3'
	5'-GGTGAGGAGCACGTAGTCGG-3'
Mouse CCL2	5'- ACGCCCCACTCACCTGCTG-3'
	5'-CCTGCTGCTGGTGATCCTCTTG-3'
Mouse IL-6	5'-GCCTTCTTGGGACTGATGCT-3'
	5'-GGTCTGTTGGGAGTGGTATCC-3'
Mouse LOX-1	5'-AAGATGAAGCCTGCGAATGACGAG-3'
	5'-ACACCAGGCAGAGGATGACCAG-3'
Mouse FATP2	5'-GGAACCACAGGTCTTCCAAA-3'
	5'-TAAAGTAGCCCCAACCACGA-3'
Mouse BMAL1	5'-CTCCAGGAGGCAAGAAGATTC-3'
	5'-ATAGTCCAGTGGAAGGAATG-3'
Mouse Lipe	5'-AACTCCTTCCTGGAACTAAG-3'
	5'-CTTCTTCAAGGTATCTGTGC-3'
Mouse LOX-1 promoter	5'-TGGACTGGATGGTTCGACTTG-3'
	5'-ACTCAGGGCCAGGAATGGAA-3'

Table S4. QC metrics for the RNA-seq data.

Sample	raw_reads	raw_bases	clean_reads	clean_bases	valid_bases	Q30	GC	Total mapped reads	Uniquely mapped
ApoE1	57.57M	8.64G	56.77M	8.06G	93.3%	95.54%	50.42%	56008857(98.65%)	50792134(89.46%)
ApoE2	55.88M	8.38G	55.12M	7.84G	93.59%	95.59%	50.9%	54379283(98.65%)	50108049(90.90%)
ApoE3	54.41M	8.16G	52.80M	7.35G	90.04%	91.14%	50.82%	51996454(98.47%)	46979689(88.97%)
KO1	53.01M	7.95G	52.20M	7.47G	93.9%	95.28%	50.13%	51471056(98.61%)	47573941(91.15%)
KO2	54.09M	8.11G	53.34M	7.61G	93.81%	95.58%	50.95%	52631363(98.66%)	48959442(91.78%)
KO3	57.08M	8.56G	56.30M	8.08G	94.38%	95.44%	50.61%	55510843(98.59%)	51602334(91.65%)
KO4	53.11M	7.97G	52.32M	7.45G	93.51%	95.48%	51.05%	51553451(98.53%)	47854627(91.46%)

raw_reads: Number of original reads

raw_bases: Number of bases

clean_reads: Number of clean reads obtained after pretreatment

clean_bases: Number of bases obtained after pretreatment

valid_bases: Percentage of effective bases

Q30: The percentage of bases with a Qphred value more than 30 in raw_bases to the total bases

GC: The percentage of the total number of G and C in clean bases to the total number of bases

Total mapped reads: Number of sequences that can be mapped to the genome

Uniquely mapped: Number of sequences with unique alignment positions on the reference sequence

Table S5. Blood pressure and heart rate in Ang II-infused mice.

Groups	sBP(mmHg)	dBP(mmHg)	HR(Beats/min)
ApoE$^{-/-}$	105.1±1.6	57.9±3.3	457.1±15.6
ApoE$^{-/-}$+Ang II	141.3±3.3*	91.3±3.6*	440.8±16.6
ApoE$^{-/-}$Nur77$^{-/-}$	106.5±1.6	63.0±2.9	449.5±23.5
ApoE$^{-/-}$Nur77$^{-/-}$ +Ang II	145.7±4.1$^{\#}$	91.2±2.5$^{\#}$	463.1±21.5

N is 4-5 in each group. Data are expressed by mean ± SD.

*P<0.05 compared to control ApoE$^{-/-}$ mice

$^{\#}$P<0.05 compared to ApoE$^{-/-}$+Ang II mice

Table S6. Blood pressure and heart rate in Celastrol-treated mice.

Groups	sBP(mmHg)	dBP(mmHg)	HR(Beats/min)
Sham + Veh	104.3±3.6	53.7±4.9	446.1±18.9
Sham + Cel	104.8±2.7	60.3±7.1	441.8±29.5
AAA + Veh	147.3±5.8*	92.1±3.4*	463.9±29.8
AAA + Cel	146.7±3.2#	92.3±1.9#	438.1±24.0

N is 4-5 in each group. Data are expressed by mean ± SD.

*P<0.05 compared to control Sham+ Veh mice

#P<0.05 compared to control AAA+ Veh mice

Figure S1. Physiological condition of different groups.
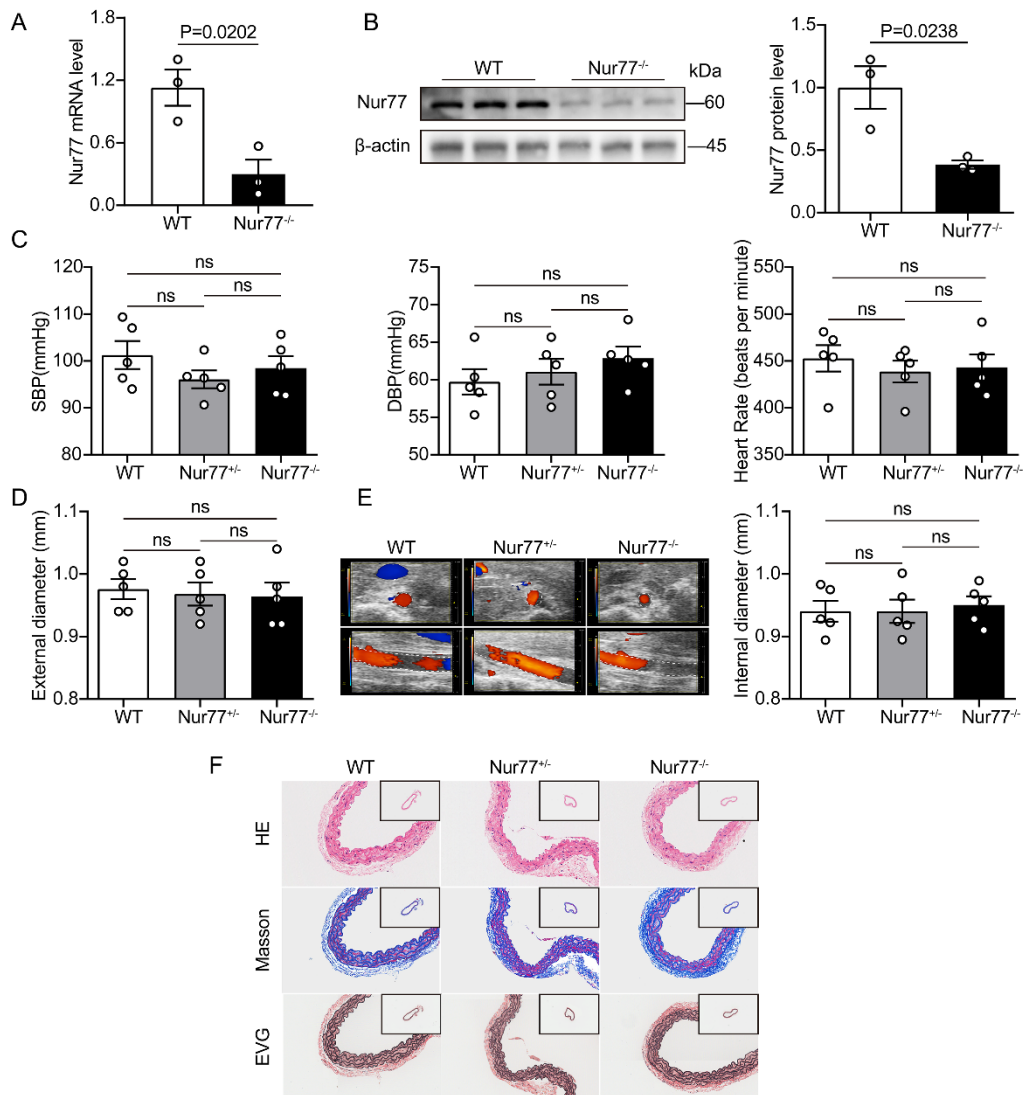
A and B, The relative mRNA and protein levels of Nur77 in WT and Nur77$^{-/-}$ group (n=3 mice per group). **C,** SBP, DBP, and Heart rate in the indicated groups (n=5 mice per group). **D,** The external diameter of abdominal aortas measured with vernier calipers in the indicated groups (n=5 mice per group). **E,** The internal diameter of abdominal aortas measured with ultrasonography (n=5 mice per group). **F,** Representative images of suprarenal aortic sections stained with hematoxylin and eosin (H&E), Masson Trichrome (collagen) and Van Gieson (elastin). Data are presented as mean± SEM. Student's two-tailed t test for A, B; one way-ANOVA followed by Tukey's multiple comparisons test for C, D. ns, nonsignificant; WT, wild type; SBP, systolic blood pressure; DBP, diastolic blood pressure.

Figure S2. Representative immunofluoresence and immunohistochemical images.
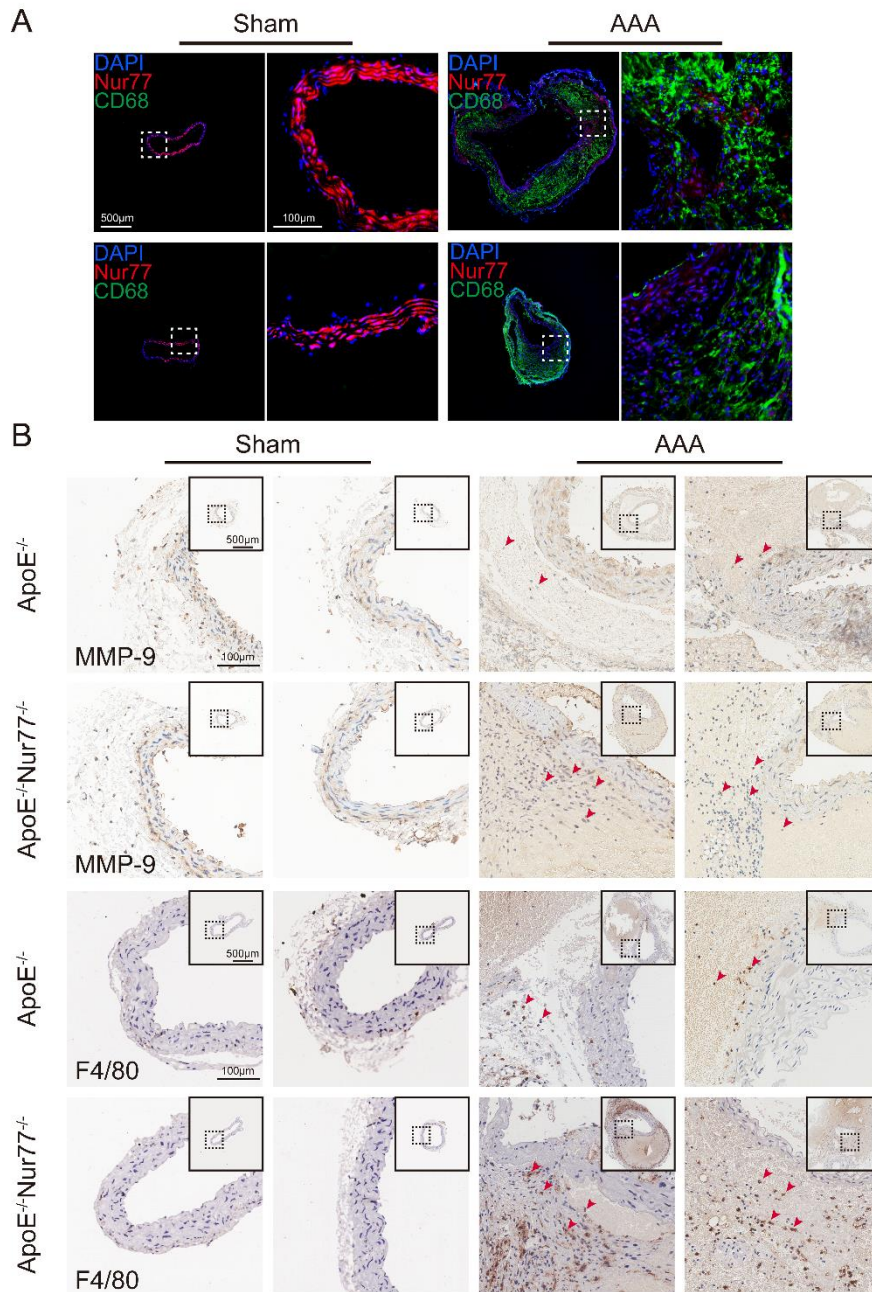
A, Representative images of dual immunofluorescence staining of Nur77 (red) and CD68 (green) in the abdominal aorta tissue from mice with AAA and sham control. **B,** Representative immunohistochemical staining images showing macrophages (F4/80) and MMP-9 in mouse abdominal aortas. AAA, abdominal aortic aneurysm; MMP, matrix metalloproteinase.
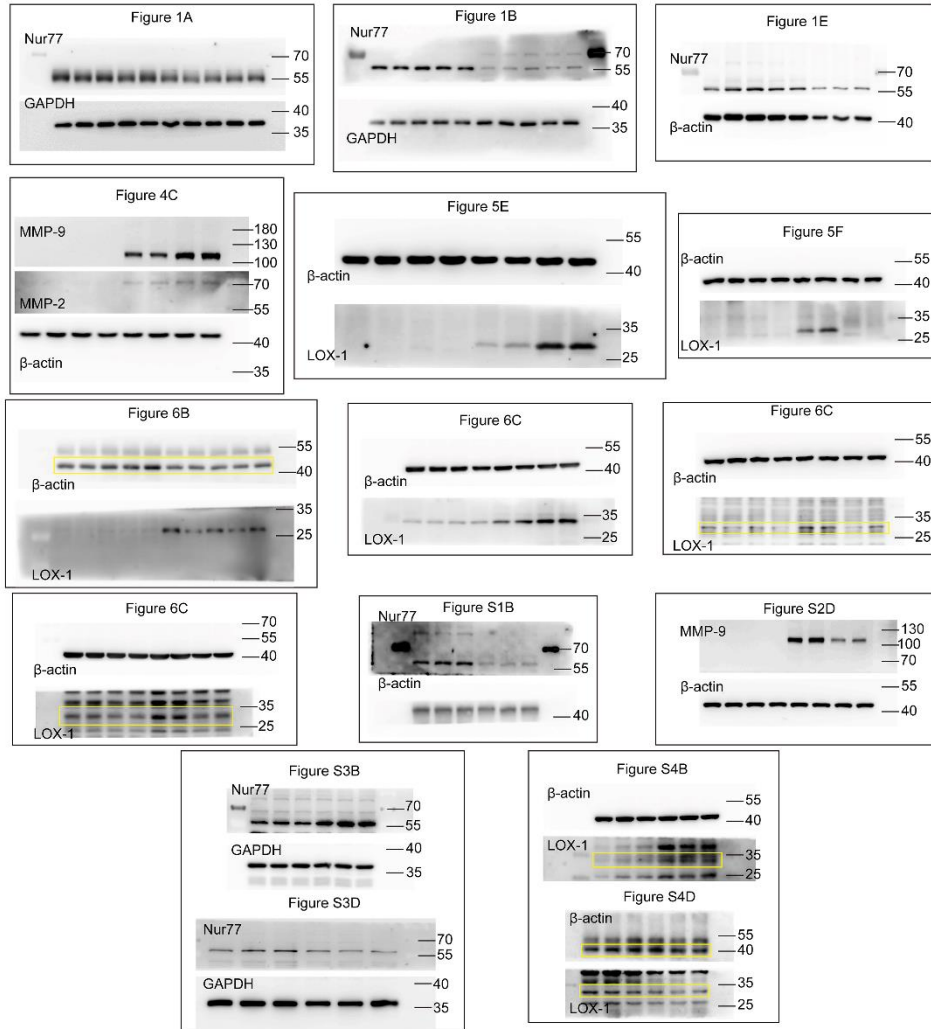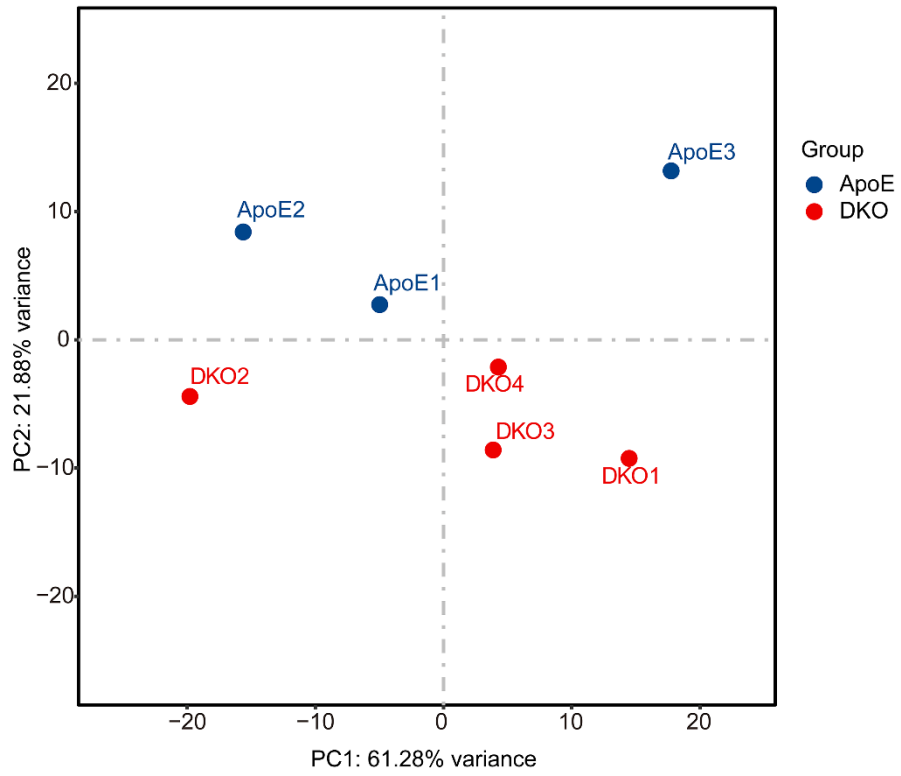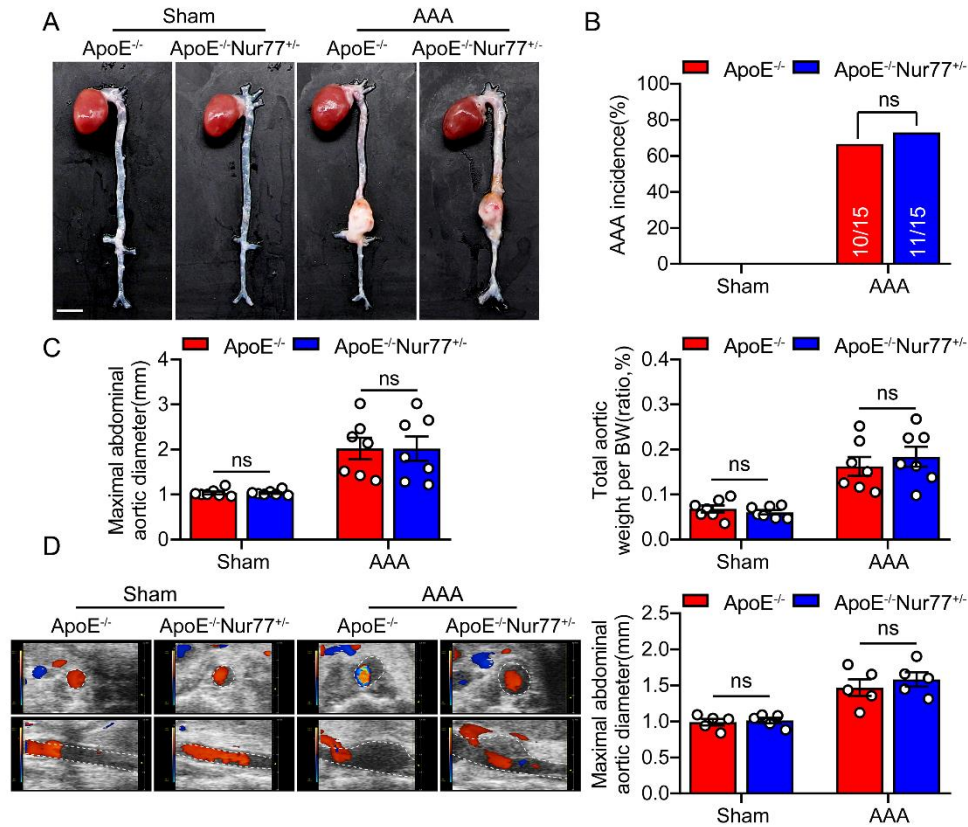
Figure S3. Full blots of the Western data

Figure S4. **Principal component analysis of the RNA-seq data**

ApoE:ApoE$^{-/-}$ mice; DKO: ApoE$^{-/-}$Nur77$^{-/-}$ mice

Figure S5. Characteristics of abdominal aortic aneurysm in ApoE$^{-/-}$ Nur77$^{+/-}$ mice.

ApoE$^{-/-}$ and ApoE$^{-/-}$Nur77$^{+/-}$ mice were subjected to AAA surgery. **A,** Representative photographs showing mouse aortas infused with saline or Ang II at 4 Weeks. Scale bar indicates 5mm. **B,** The incidence of AAA of the Ang II-infused mice compared with their sham controls. n=10 in each group of ApoE$^{-/-}$, ApoE$^{-/-}$Nur77$^{+/-}$ mice infused with saline, n=15 each for ApoE$^{-/-}$, ApoE$^{-/-}$Nur77$^{+/-}$ mice infused with Ang II. **C,** Maximal abdominal aortic diameter, total aortic weight-to-BW ratio of the indicated groups (n=7). **D,** Representative views of the internal diameter of the abdominal aorta measured with ultrasonography and the quantification of the maximal abdominal aortic diameter (n=5). Data are presented as mean± SEM. Fisher's exact test for B. Two-way ANOVA followed by Tukey's multiple comparisons test for C and D. ns, nonsignificant; AAA, abdominal aortic aneurysm; BW, body weight.

Figure S6. Celastrol attenuated the macrophages infiltration and MMP-9 expression.
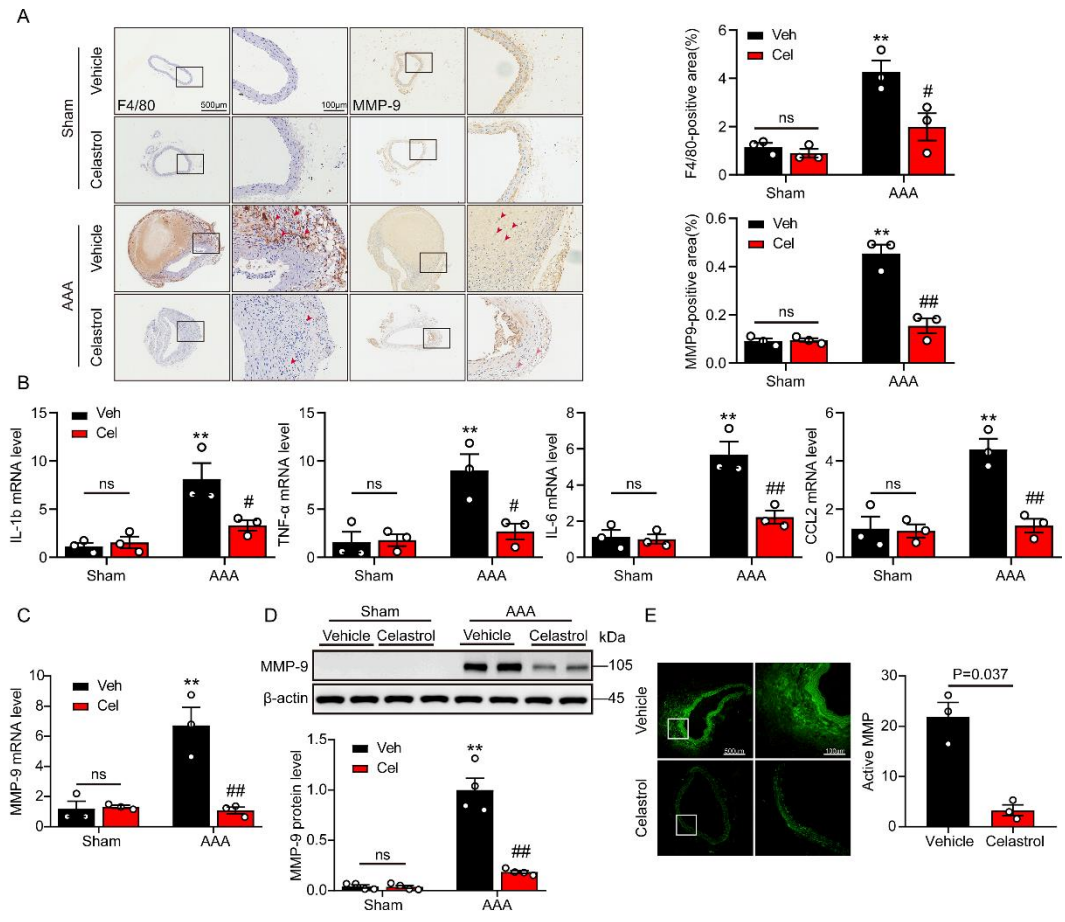
A, Representative immunohistochemical staining images showing macrophages (F4/80) and MMP-9 in mouse abdominal aortas, with the quantification results in the right panels (n=3 mice per group). **B,** The q-PCR analysis of inflammatory cytokines (IL-1b, TNF-α, CCL2, and IL-6) in the aortic wall. Results were normalized against GAPDH and converted to fold induction relative to their respective controls (n=3 mice per group). **C,** Gene expression of MMP9 in AAA lesioned tissues. Results were normalized against GAPDH and converted to fold induction relative to their respective controls (n=3 mice per group). **D,** Western blot analysis and quantitative results of MMP9. Results were normalized against tubulin and converted to fold induction relative to their respective controls (n=4 mice per group). **E,** In situ zymography for gelatinase activity (n=3 per group). $^{*}P<0.05$ vs Sham-vehicle mice, $^{**}P<0.01$ vs Sham-

vehicle mice; [#]P<0.05 vs AAA-vehicle mice, [##]P<0.01 vs AAA-vehicle mice. Data are presented as mean± SEM. Two-way ANOVA followed by Tukey's multiple comparisons test for A-D. Student's two-tailed t test for E. ns, nonsignificant; Veh, vehicle; Cel, celastrol; IL-1b, Interleukin-1β; TNFα, tumor necrosis factor-α; CCL2, chemokine (C-C motif) ligand 2; IL-6, Interleukin-6; MMP, matrix metalloproteinase.

**Figure S7. The expression level of Nur77.**
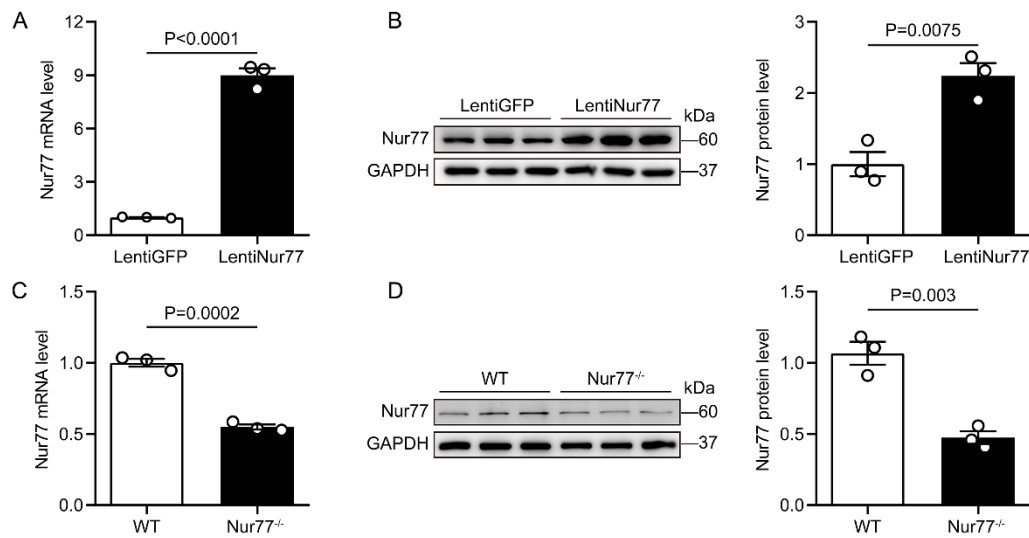
A and B, The expression of Nur77 in Raw264.7 cells transduced with LentiGFP or LentiNur77 to overexpress Nur77. The mRNA level (A) or the protein level (B) of Nur77 (n=3 independent experiments per group). **C and D,** The expression of Nur77 in bone marrow-derived macrophages (BMDMs) from WT or Nur77$^{-/-}$ mice. The mRNA level (C) or the protein level (D) of Nur77 (n=3 independent experiments per group). Data are presented as mean± SEM. Student's two-tailed t test for A-D. Lenti, lentiviral; GFP, green fluorescent protein; WT, wild type.

Figure S8. The expression level of LOX-1.
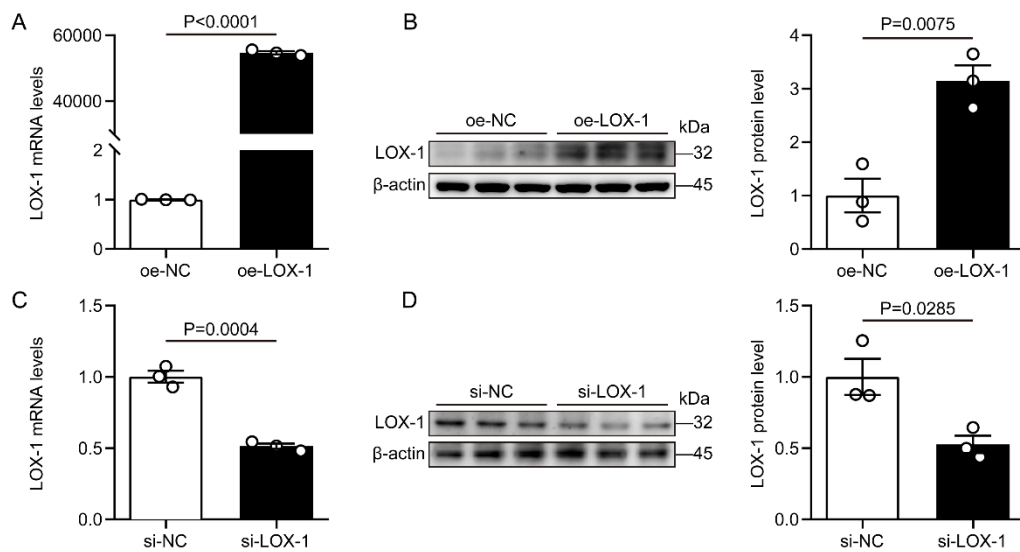
A and B, The expression of LOX-1 in Raw264.7 cells transduced with LOX-1 overexpression plasmid (oe-LOX-1) to overexpress LOX-1. The mRNA level (A) or the protein level (B) of LOX-1 (n=3 independent experiments per group). **C and D,** The expression of LOX-1 in BMDMs transfected with control siRNA(si-NC) or LOX-1 siRNA(si-LOX-1). The mRNA level (C) or the protein level (D) of Nur77 (n=3 independent experiments per group). Data are presented as mean± SEM. Student's two-tailed t test for A-D. BMDM, bone marrow-derived macrophage; LOX-1, lectin like Ox-LDL receptor-1; oe, overexpression; si, small interfering RNA.

Figure S9. Expression of Nur77 in vascular smooth muscle cells in AAA.
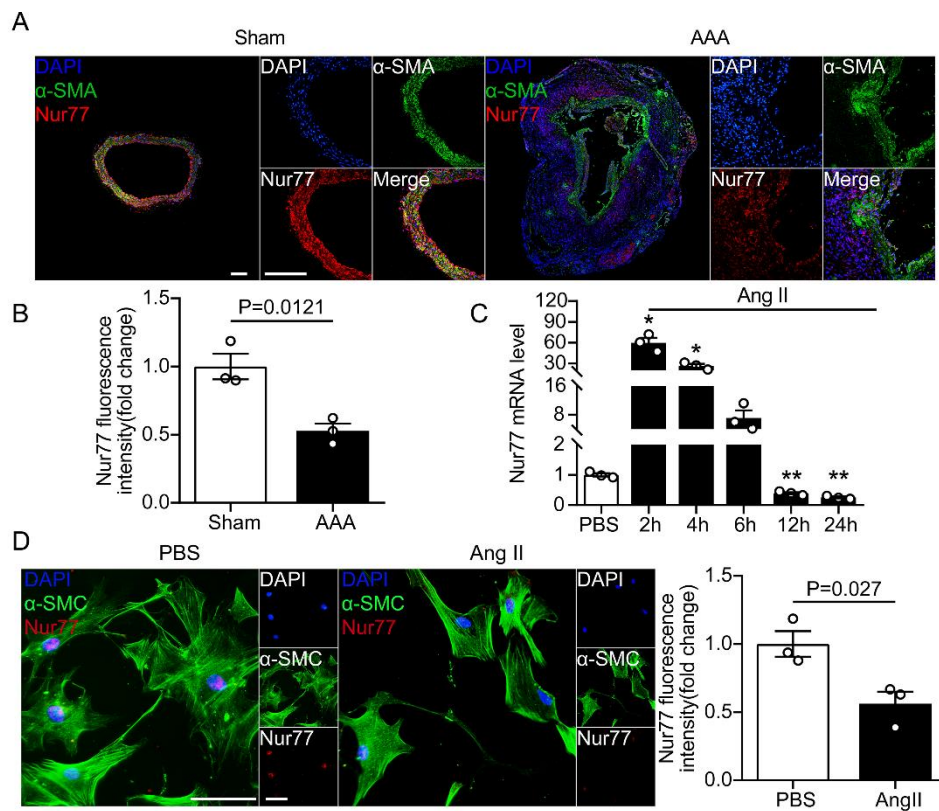
A, Representative images of dual immunofluorescence staining of Nur77 (red) and α-SMA (green) in the abdominal aorta tissue from mice with AAA and sham control (n=3 per group). Scale bar indicates 200μm. **B,** Quantification of the relative Nur77 fluorescence intensity in aortas from mice with AAA and sham control. **C,** The relative mRNA level of Nur77 in Movas cells after stimulated with Ang II (1μM) for the indicated time (n=3 per group, *P<0.05 vs PBS, **P<0.01 vs PBS). **D,** Representative images of dual immunofluorescence staining of Nur77 (red) and α-SMA (green) in Movas cells, and quantification of the relative Nur77 fluorescence intensity. Scale bar indicates 200μm. Data are presented as mean± SEM. Student's two-tailed t test for B and D. One way-ANOVA followed by Dunnett's T3 multiple comparisons test for C. AAA, abdominal aortic aneurysm; Ang II, angiotensin II; α-SMA, alpha smooth muscle actin.